Adaptation of Whisker Movements Requires Cerebellar Potentiation

Vincenzo Romano[1,5], Licia De Propris[1,2,5], Laurens W.J. Bosman[1,5,*], Pascal Warnaar[1], Michiel M. ten Brinke[1], Sander Lindeman[1], Chiheng Ju[1], Arthiha Velauthapillai[1], Jochen K. Spanke[1], Emily Middendorp Guerra[1], Tycho M. Hoogland[1,2], Mario Negrello[1], Egidio D'Angelo[3,4] and Chris I. De Zeeuw[1,2,*]

[1]Department of Neuroscience, Erasmus MC, Rotterdam, 3000 CA, the Netherlands

[2]Netherlands Institute for Neuroscience, Royal Academy of Arts and Sciences, Amsterdam, 1105 BA, the Netherlands

[3]Department of Brain and Behavioral Sciences, University of Pavia, Pavia, 27100, Italy

[4]Brain Connectivity Center, Instituto Fondazione C. Mondino, Pavia, 27100, Italy

[5]These authors contributed equally.

[*]Correspondence to: Chris I. De Zeeuw (Lead Contact), Department of Neuroscience, PO Box 2040, 3000 CA Rotterdam, the Netherlands, c.dezeeuw@erasmusmc.nl or Laurens W.J. Bosman, Department of Neuroscience, PO Box 2040, 3000 CA Rotterdam, the Netherlands, l.bosman@erasmusmc.nl

Summary

The ability to adapt while exploring the world is critical for survival, yet how it comes about is unclear. Here we show that a whisker protraction reflex can be elicited following rostro-caudal pad stimulation, and that short-term kinematics of this reflex are enhanced when coherent complex spike activity of cerebellar Purkinje cells occurs in *crus 1*. Instead, the long-term kinematics can be adapted by tetanic stimulation and this adaptation is largely controlled by changes in the simple spike activity of Purkinje cells in *crus 2*. Increases in whisker protraction correlate with preceding increases in simple spikes in trial-by-trial variation analysis, and both behavioral and spike adaptation are absent in independent mouse models in which postsynaptic long-term potentiation of Purkinje cells is blocked. These differentially distributed short-term and long-term cerebellum-dependent modulations of whisker movements may come into play during coordination and adaptation of natural behaviors like gap crossing and prey capture.

Impact statement

Romano et al. show direct coupling between increased cerebellar activity and motor learning, with both phenomena being absent in independent mouse models lacking parallel fiber LTP.

Introduction

Active touch is important for exploring our environment, allowing us to assess the shape, substance and movements of objects and organisms around us (Prescott et al., 2011). Throughout the animal kingdom, various systems have evolved for this purpose; these include for example the antennae of insects, the fingertips of primates and the well-developed whisker systems of rodents and sea mammals (Ahl, 1986; Dehnhardt et al., 2001; Staudacher et al., 2005; Dere et al., 2007; Anjum and Brecht, 2012). Controlling and adapting movements of such systems are thus critical in both daily life and life-threatening situations. Whereas the role of the cerebral cortex in the planning and initiation of active touch is relatively well established (Kleinfeld et al., 1999; Brecht, 2007; Bosman et al., 2011; Petreanu et al., 2012; Diamond and Arabzadeh, 2013; Feldmeyer et al., 2013; Guo et al., 2014; Petersen, 2014; Deschênes et al., 2016), that of the cerebellum in learning how to adapt these movements is less clear (Popa et al., 2012; Chen et al., 2016, 2017). Conceptually, the cerebellum may generate representations to predict the sensory consequences of active control (Wolpert et al., 1998; Medina and Lisberger, 2007; Brooks et al., 2015; Streng et al., 2018), but with which cellular and network mechanisms it may adjust such representations remains to be elucidated. In the past, long-term depression (LTD) at the parallel fiber-to-Purkinje cell (PC) synapse, guided by climbing fiber activity, has been considered to be the main cellular mechanism underlying cerebellar motor learning (Albus, 1971; Konnerth et al., 1992; Ito, 2003; Koekkoek et al., 2003; Medina and Lisberger, 2008). Parallel fiber LTD is, however, not the sole mechanism underlying cerebellar plasticity. Recently, short-term adaptation of movements could be linked to a bidirectional change in simple spike firing, depending on the presence or absence of climbing fiber activity during the previous trial (Yang and Lisberger, 2014; Herzfeld et al., 2018). Moreover, recent evidence suggests that also long-term

potentiation (LTP) of the parallel fiber-to-PC synapse is behaviorally relevant (Schonewille et al., 2010; Schonewille et al., 2011; Rahmati et al., 2014; Gutierrez-Castellanos et al., 2017; Voges et al., 2017), although direct electrophysiological evidence that cerebellar LTP can underlie long-term behavioral changes on a trial-by-trial basis is still largely lacking.

To study the potential impact of long-term synaptic plasticity in PCs on the control of motor output, we elaborated on recent findings showing that ongoing whisker movements in mice can be reflected in PC simple spike firing (Proville et al., 2014; Chen et al., 2016). Mice, like rats, sweep their whiskers rhythmically while exploring the environment and they adapt these movements to the changing sensory stimuli (Welker, 1964; Ahl, 1986; Berg and Kleinfeld, 2003; Voigts et al., 2015). We hypothesized that, as shown for other forms of motor learning like eyeblink conditioning (Jirenhed et al., 2007; Ten Brinke et al., 2015), adaptation of the vestibulo-ocular reflex (Schonewille et al., 2010; Voges et al., 2017) and adjustment of smooth pursuit or saccadic eye movements (Thier et al., 2002; Catz et al., 2008; Medina and Lisberger, 2008; Herzfeld et al., 2014; Yang and Lisberger, 2014; Herzfeld et al., 2015; Yang and Lisberger, 2017; Herzfeld et al., 2018), plasticity at the level of the PC network may contribute to entrainment of modified whisker movements.

As cerebellar training protocols for whisker movements had not been developed, we designed a novel paradigm. We based the induction protocol on the known dynamics at the cerebellar input stage, the granular layer, which indicate that sensory stimulation at theta band frequencies – in particular at 4 Hz – may be particularly efficient in inducing plasticity (D'Angelo et al., 2001; Lev-Ram et al., 2002; Lev-Ram et al., 2003; Coesmans et al., 2004; Ramakrishnan et al., 2016). In view of the predominantly positive correlation between simple spike firing and the set point of the whiskers (Chen et al., 2016), we expected that 4 Hz tetanic stimulation of the whisker pad in rostro-caudal direction would lead to a concomitant change in whisker protraction and simple spike firing. We show that in naïve untrained animals,

modulatory activity of the climbing fibers in predominantly *crus 1* precedes reflexive whisker movements following rostro-caudal stimulation of the pad, while that of the simple spikes occurs at the same time as the whisker movements. Instead, after induction of the training protocol with tetanic stimulation in the same direction enhanced simple spike modulation in predominantly *crus 2* that anticipates increased whisker protraction, which can be prevented by blocking LTP at the parallel fiber-to-PC synapse. These data indicate that reflexive and adaptive whisker movements can be mediated by short-term and long-term control of complex spike and simple spike activity, respectively, and that these processes can be distributed among different Purkinje cells.

Results

Whisker pad stimulation triggers stereotypic whisker behavior

The large facial whiskers are a prime source of sensory information for many mammals, in particular for rodents that can make elaborate movements with their large facial whiskers (Welker, 1964; Brecht, 2007; Bosman et al., 2011; Arkley et al., 2017). It has been noted that passive touch can trigger active whisker movements in mice (Ferezou et al., 2007), but this behavior has not been described in great detail yet. Here, we studied whisker movements following rostro-caudal air puff stimulation of the whisker pad in 16 awake, head-restrained mice (Figure 1A-C). Under these conditions, with a 2 s inter-trial interval, spontaneous whisking in between stimuli was rare: only in 12% of all trials whisker movements of more than 10° happened during the 200 ms prior to an air puff to the whisker pad. An air puff in rostro-caudal direction induced a passive backward movement that was typically followed by a stereotypic large protraction, exceeding 10° in amplitude in 82% of all trials. After this touch-evoked protraction, whisker behavior was more variable with prolonged whisker movements (>200 ms) being observed in approximately half (51%) of the trials (Figure 1D-H). In the other half of the trials, movement stopped after returning to the resting position directly following the first protraction. The puffer was placed in such a way that most, if not all, large mystacial whiskers were affected by the air flow. The touch-evoked protraction was typically performed by all whiskers simultaneously (*data not shown*). We conclude that mechanical stimulation in rostro-caudal direction triggers a synchronized forward sweep of all large facial whiskers in most trials, which is followed by a prolonged period of active whisking in half of the trials.

Air puffs induce reflexive whisker movements

To understand the nature of touch-evoked whisker movements, we varied the stimulus conditions. We reasoned that if the air puff triggered a conscious, explorative movement, the animal would most likely make a movement towards the source of the air puff. To this end, we placed a second air puffer at the caudal side of the whisker field and a third air puffer at the front of the contralateral whisker field. A startle response would be expected to be more stereotypic, involving less direction-specificity and it should be suppressed by a brief pre-pulse (Gogan, 1970; Swerdlow et al., 1992; Moreno-Paublete et al., 2017). During a single recording session, air puffs from the three different orientations were given and intermingled with trials including a brief pre-pulse, all in a random order (Figure 2A). Irrespective of the direction of the stimulus, a reflexive forward sweep was triggered, providing an argument against this being a conscious, explorative movement (Figure 2B-C). An air puff from the front on the ipsilateral side induced a largely passive retraction prior to the stereotypic protraction. Such a retraction was largely absent when stimulating from the back and of shorter duration when giving a brief pre-pulse. Contralateral stimulation also evoked a slight retraction, followed by a much larger forward sweep (Figure 2B-E; Table S1). The absence of a diminishing effect of the weaker pre-pulse on the reaction to the stronger pulse (p = 0.268; Dunn's pairwise post-hoc test after Friedman's ANOVA; p = 0.003; Fr = 13.933; df = 3) as well as the finding that the subsequent strong pulse did not evoke a larger protraction than the preceding weak pre-pulse (p = 0.496, Wilcoxon-matched pairs test; Figure 2B inset) led us to conclude that the touch-evoked whisker protraction is unlikely reflecting a startle response (Figure 2E; Table S1). Altogether, the stereotypic nature of the touch-evoked whisker movements in the absence of indications for a startle response indicates that this is a reflexive movement.

Anatomical distribution of Purkinje cell responses to whisker pad stimulation

Modulation of reflexive movements requiring sensorimotor integration is a well-established function of the cerebellum, as has been extensively studied for instance in eyeblink conditioning (Alba et al., 1994; Christian and Thompson, 2003; Heiney et al., 2014; Ten Brinke et al., 2015) and oculomotor reflexes (Lisberger and Fuchs, 1978; Waespe et al., 1985; Medina and Lisberger, 2008; Schonewille et al., 2011; Yang and Lisberger, 2014; Herzfeld et al., 2018). Accordingly, PCs receive sensory whisker input not only directly from the brainstem but also indirectly from thalamo-cortical pathways (Kleinfeld et al., 1999; Bosman et al., 2011; McElvain et al., 2018) and the dynamics of their responses upon whisker stimulation are heterogeneous (Brown and Bower, 2001; Loewenstein et al., 2005; Bosman et al., 2010; Chu et al., 2011) (Figure 3F). We first mapped the firing properties of PCs in the ipsilateral lobules *crus 1* and *crus 2* in response to whisker pad air puff stimulation in awake mice. Of the 132 single-unit PCs from which we recorded, 118 (89%) showed significant complex spike responses, but with large variations in latency and amplitude (Figure 3A-C, Figure 3 – figure supplement 1A-B). Following cluster analysis of the strength of their responses PCs could be split in two groups. A subset of PCs could be classified as “strong complex spike responders” (45 PCs, i.e., 34%), while most PCs that were responsive to whisker stimulation were classified as “weak complex spike responders” (87 PCs, i.e., 66%) (Figure 3 – figure supplement 1D-F).

Significant simple spike responses were found in 127 (96%) of the 132 recorded PCs. Simple spike responses were often bi-phasic, consisting of a period of inhibition followed by one of excitation, or vice versa (Figures 3D-E, Figure 3 – figure supplement 1C). The trough of the simple spike responses typically correlated in a reciprocal fashion with the peak of the complex spike responses (Figures 3A-E; Figure 3 – figure supplement 1A-C) (De Zeeuw et al., 2011; Badura et al., 2013; Zhou et al., 2014).

To chart the spatial distribution of the PCs with different response kinetics upon whisker stimulation we combined electrolytic lesions (Figure 3G) with reconstructions of the electrode entry points, generating a map of the recording locations of the 132 PCs recorded with the quartz/platinum electrodes. Complex spike responses to whisker stimulation were found to be especially strong in the lateral zones of *crus 1* (Figure 3H) and the first phase of the simple spike responses were found to be largely reciprocal: in areas where complex spike responses were strong, simple spikes were mainly suppressed, and vice versa they were predominantly facilitated in the cells where complex spike responses were weak (Figure 3H-I; Figure 3 – Figure supplement 1G-H).

Next, we verified this distribution by using double-barrel glass pipettes with which we injected neural tracer, BDA 3000, at the recording spot after recording. Following identification of the source of the climbing fibers in the inferior olive and the projection area in the cerebellar nuclei (Figure 3 – Figure supplement 2A-C) we defined the cerebellar area in which the recorded PC was located (cf. (Voogd and Glickstein, 1998; Apps and Hawkes, 2009). These experiments confirmed that the strong complex spike responders were situated most prominently in the lateral part of *crus 1*, whereas most cells in *crus 2* were weak complex spike responders (Figure 3 – Figure supplement 2D). In conclusion, following whisker stimulation we could identify a region with predominantly strong complex spike and inhibitory simple spike responses in the lateral part of *crus 1*, whereas *crus 2* contained more PCs with a weak complex spike and facilitating simple spike response, respectively.

Coherent complex spike firing is specifically enhanced by whisker pad stimulation

Next, we used two-photon Ca^{2+} imaging to study the behavior of adjacent groups of PCs around the moment of whisker pad air puff stimulation in awake mice. After injection of the Ca^{2+}-sensitive dye Cal-520 we could recognize the dendrites of PCs as parasagittal stripes

(Figure 4A), each of which showed fluorescent transients at irregular intervals (Figure 4B). Previous studies identified these transients as the result of PC complex spike firing (Schultz et al., 2009; Tsutsumi et al., 2015). Occasionally, signals could be found that were shared by many PCs, even in the absence of sensory stimulation (Figure 4B) in line with earlier reports (Mukamel et al., 2009; Ozden et al., 2009; Schultz et al., 2009; De Gruijl et al., 2014). Upon whisker pad stimulation, complex spike firing occurred much more often collectively in multiple Purkinje cells (Figure 4C). To quantify this form of coherent firing, we counted the number of complex spikes fired per frame (of 40 ms) and determined the level of coherence using cross-correlation analyses (Figure 4D). The levels of coherence increased to such strength that they were extremely unlikely to have occurred by the increase in firing frequency alone (compared to a re-distribution of all events based on a Poisson distribution; Figure 4E). In other words, firing of a single or a few PCs was the dominant mode of activity in the absence of stimulation, and this changed towards the involvement of many PCs upon stimulation, firing coherently (Figure 4F-G). We conclude that groups of adjacent PCs in *crus 1* respond to whisker pad stimulation by increased complex spike firing with an enhanced level of coherence.

Larger whisker protractions are preceded by complex spikes

In view of the strong convergence between PCs and cerebellar nuclei neurons, we expect that complex spike coherence may contribute to driving motor activity (Mukamel et al., 2009; Hoogland et al., 2015). To study the impact of complex spike firing on touch-evoked whisker protraction, we segregated the trials during which a complex spike was fired by a single PC from those during which no complex spike was produced. It turned out that during the trials with a complex spike, the protraction was significantly larger (see Figure 5A for a single PC; Figure 5B for the population of 55 PCs that responded to air puff stimulation). A direct

comparison between the timing of the complex spike response and the difference in whisker position between trials with and without a complex spike revealed that the peak in complex spike preceded the moment of maximal difference in position after stimulation by 63 ± 4 ms (mean ± SEM; n = 55; Figure 5C-D). The maximal difference in protraction contributed by a complex spike equaled 0.80° (median, with IQR of 2.80°; $p < 0.001$), whereas this was only 0.28° (0.92°) for retraction (p = 0.002; Wilcoxon matched pairs tests, significant after Bonferroni correction for multiple comparisons: $\alpha = 0.05/3 = 0.017$) (Figure 5E).

Instantaneous simple spike firing correlates with whisker protraction during reflex

The firing rate of simple spikes has been shown to correlate with whisker position: in the large majority of PCs, simple spike firing is correlated with protraction and in a minority it correlates with retraction (Chen et al., 2016). This led us to study the correlation in simple spike firing during touch-induced whisker protraction. At first sight, variation in simple spike firing roughly correlated to periods with whisker movement (Figure 6A-B). To study this in more detail, we made use of the inter-trial variations in simple spike rate and whisker position, allowing us to make a correlation matrix between these two variables on a trial-by-trial basis (cf. (Ten Brinke et al., 2015). In a representative example (Figure 6C), the whisker protraction and peak in simple spike firing were roughly simultaneous. In the correlation matrix, this is visualized by the yellow color along the 45° line. This turned out to be the general pattern in 25 of the 56 PCs (45%) of which we had electrophysiological recordings during whisker tracking (Figure 6D). In all of these 25 PCs, there was a positive correlation between instantaneous simple spike firing and whisker protraction that occurred relatively late during the movement, in particular between 80 and 200 ms after the start of the stimulus (Figure 6C-D; Figure 6 – Figure supplement 1C), thus well after the complex spike responses occurred (Figure 5C). In the 31 remaining PCs, the ones that did not display a significant

correlation when evaluated at the level of individual cells, we still observed a correlation at the population level. Remarkably, this correlation was negative, i.e. showing a correlation between simple spike firing and retraction (Figure 6 – Figure supplement 1). We conclude that during the touch evoked whisker reflex simple spikes predominantly correlate with whisker protraction and that this correlation is maximal without a clear time lead or lag, unlike the complex spikes whose occurrence tended to precede the protraction.

Contralateral whisker pad stimulation induces stronger whisker protraction and stronger simple spike responses

If an increase in simple spike firing correlates to stronger whisker protraction, then the simple spike response to contralateral stimulation should be larger than that to ipsilateral stimulation, as contralateral stimulation evokes a stronger protraction (Figures 2 and 7A). To test this we recorded PC activity while stimulating the ipsi- and contralateral whiskers in a random sequence (Figure 7B). The change in maximal protraction was considerable (difference in maximal protraction: 7.30 ± 1.24° (mean ± SEM); n = 9 mice; Figure 7C; cf. Figure 2E). Possibly, the absence of direct impact of the air flow during contralateral stimulation can explain part of this difference, which is also in line with the earlier onset of the protraction during contralateral stimulation (Figure 7C). However, in addition to this passive process, a change in simple spikes may actively contribute to this difference as well, as the simple spikes increased significantly more during contralateral stimulation (increase during first 60 ms after air puff onset for contra- vs. ipsilateral stimulation: 13.7 ± 5.3%; mean ± SEM; p = 0.023; t = 2.413; df = 26; paired t test; n = 27 PCs; Figure 7E). Instead, the complex spike response was reduced during contralateral stimulation (complex spike peak response: ipsilateral: 1.40% (1.25%); contralateral: 0.71% (0.81%); medians (IQR); p < 0.001; Wilcoxon matched-pairs test; n = 27 PCs) (Figure 7D).

Simple spikes have been shown not to initiate but to modulate ongoing whisker movements (Proville et al., 2014; Chen et al., 2016). To find out whether simple spike firing could modulate touch-evoked whisker protraction, we investigated the impact of artificial activation of PCs by optogenetic stimulation. To this end we used L7-Ai27 mice, which express channelrhodopsin-2 exclusively in their PCs and show a strong increase in their simple spike firing upon stimulation with blue light (Witter et al., 2013). We placed an optic fiber of 400 µm diameter at the *crus 1/2* region and compared air puff-induced whisker movements between trials with and without 100 ms of optogenetic PC stimulation. As expected, the whisker protraction was larger during the trials with optogenetic stimulation when simple spike firing in the PCs was increased ($p < 0.001$; $t = 4.411$; df = 12; paired t test; $n = 13$ mice; Figure 7 – Figure supplement 1). Taken together, increased simple spike firing can be correlated to stronger whisker protraction, whether evoked by contralateral whisker stimulation or by direct optogenetic stimulation.

Tetanic 4 Hz stimulation leads to acceleration of the simple spike response and to stronger protraction of the whiskers

Next, we investigated whether sensory experience could modulate the touch-evoked whisker protraction, the frequency of simple spike firing and the relation between them. We hypothesized that whisker movements might be enhanced following tetanic stimulation at 4 Hz, as this frequency has been shown to be particularly effective in inducing potentiation at the parallel fiber-to-PC synapse (D'Angelo et al., 2001; Lev-Ram et al., 2002; Coesmans et al., 2004; Ramakrishnan et al., 2016). Indeed, application of this 4 Hz tetanic stimulation to the whisker pad for only 20 seconds was sufficient to induce an increase in the maximal protraction (average increase 17.9 ± 3.9%; mean ± SEM; $p < 0.001$; Wilcoxon-matched pairs test; $n = 16$ mice; Figure 8A-B; Table S2).

This change in the amplitude of the touch-evoked whisker protraction was not accompanied by any substantial change in the complex spike response to whisker pad stimulation (p = 0.163; Wilcoxon matched pairs test; n = 55 PCs; Figure 8C; Table S2). However, the rate of simple spike firing upon air puff stimulation was markedly increased after 20 s of 4 Hz stimulation. This was especially clear during the first 60 ms after the air puff (p = 0.003; Wilcoxon matched pairs test; n = 55 PCs; Figure 8D; Table S2). Overlaying the averaged whisker traces and response spike profiles highlighted the earlier occurrence of facilitation in simple spike firing after the 4 Hz tetanic stimulation protocol (Figure 8E). To study this timing effect in more detail, we repeated the trial-based correlation analysis (cf. Figure 8C-D). The moment of maximal correlation between simple spike firing and whisker position was reached faster after the 4 Hz tetanic stimulation (time of maximal correlation pre-induction: 152.1 ± 18.1 ms; post-induction: 90.7 ± 9.4 ms (means ± SEM); p = 0.020; t = 2.664; df = 13; paired t test; n = 14 PCs; Figure 8F). Indeed, the maximum correlation was found to be above the 45° line after the 4 Hz tetanic stimulation, implying that the changes in simple spike firing now preceded the whisker movement, rather than being around the same time as before the induction.

During the induction phase itself (i.e. during the 4 Hz stimulation period of 20 s), both the complex spike and simple spike responses to each air puff were weakened when comparing them with the pre-induction period at which we used 0.5 Hz stimulation. More specifically, the maximum response of the complex spikes significantly decreased from a median of 1.27% (with an IQR of 1.89%) during pre-induction to 0.52% (with IQR of 0.43%) during induction (p < 0.001; Wilcoxon matched pairs tests, n = 55 PCs). Likewise, the average spiking frequency of the simple spikes in the first 200 ms after the puff decreased from a median of 94.3 Hz (with IQR of 38.3 Hz) during pre-induction to 39.9 Hz (IQR of 22.1 Hz) during induction (p < 0.001) (Figure 8 – Figure supplement 1). Thus, we conclude

that following, but not during, a brief period of 4 Hz tetanic stimulation touch-evoked whisker protraction is increased concomitantly with an increase in simple spike firing, the latter now preceding the movement.

Tetanic 4 Hz stimulation specifically potentiates simple spike firing in PCs with weak complex spike responses

As cerebellar plasticity is bi-directional and under control of climbing fiber activity (Lev-Ram et al., 2003; Coesmans et al., 2004; Ohtsuki et al., 2009), we wanted to find out to what extent plastic changes in simple spike activity can be related to the strength of the complex spike response generated by these climbing fibers. To this end we compared for each PC the strength of the complex spike responses to whisker pad stimulation to the impact of 4 Hz tetanic stimulation on simple spike responses. As expected, we found a significant negative correlation between the strength of the complex spike response and the change in simple spike response (R = 0.311; p = 0.021; linear regression on n = 55 PCs; Figure 9A). The PCs with the strongest effect of tetanic stimulation on simple spike firing were mainly located in the lateral part of *crus 2* (Figure 9B), directly posterior to the *crus 1* area with the strongest complex spike responses (Figure 3H). We compared the location of this lateral *crus 2* area to that of the PCs with the strongest correlations between simple spike firing and whisker protraction and we found these two *crus 2* locations to match (Figure 9B-C).

The impact of 4 Hz stimulation lasted as long as our recordings lasted; at least 30 min. We separated between PCs with a weak complex spike response and those with a strong one. In line with the correlation analysis shown in Figure 9A, the former PCs expressed a potentiation of their sensory simple spike responses, whereas the latter ones did not (weak vs. strong responders: p = 0.005; F = 3.961; df = 4.424; two-way repeated measures ANOVA with Greenhouse-Geyser correction; n = 8 weak and n = 6 strong responders; Fig. 9D-F).

Likewise, the impact of this stimulation on whisker protraction also lasted throughout the recording. Although the maximal protraction angle gradually decreased towards the pre-induction level, the protraction started earlier, implying a stronger muscle force during the early phase of the touch-evoked whisker protraction, and this effect remained stable throughout our recordings (Figure 9 – Figure supplement 1). Thus, both simple spikes and whisker muscles remained affected by the 4 Hz tetanic stimulation for as long as our recordings lasted.

Expression of PP2B in Purkinje cells is required for increased protraction and simple spike firing following 4 Hz tetanic stimulation

In reduced preparations, 4 Hz tetanic stimulation of the mossy fiber/parallel fiber inputs leads to LTP of parallel fiber-to-PC synapses (Lev-Ram et al., 2002; Coesmans et al., 2004; Ramakrishnan et al., 2016). At the same time, parallel fiber LTP is inhibited by climbing fiber activity (Lev-Ram et al., 2003; Coesmans et al., 2004; Ohtsuki et al., 2009). Hence, our data appear in line with a role of parallel fiber LTP as a potential mechanism underlying the observed increase in simple spike firing upon a brief period of 4 Hz stimulation. To further test a potential role for LTP, we repeated the 4 Hz tetanic stimulation experiments in L7-PP2B mice, which lack the PP2B protein specifically in their PCs, rendering them deficient of parallel fiber-to-PC LTP (Schonewille et al., 2010) (Figure 10A). Whereas 14 out of 16 WT littermates showed increased touch-evoked whisker protraction after 4 Hz stimulation, only 3 out of 13 L7-PP2B mutant mice did ($p < 0.001$; Fisher's exact test). Accordingly, the difference in maximal protraction was significantly less in the L7-PP2B mutant mice ($p = 0.044$; $t = 2.162$; df = 19; *t* test; Figure 10B-D).

In line with the absence of increased touch-evoked whisker protraction, also the increase in simple spike firing observed in WT mice was absent in L7-PP2B mice. As the

strong complex spike responders did not show plasticity (cf. Figure 9), we compared weak complex spike responders of both genotypes. Simple spike responses were stably increased in WT PCs with a weak complex spike response following tetanic stimulation (as shown in Figure 9F), but not in those of L7-PP2B mice (effect of genotype: $p = 0.003$; $F = 4.361$; df = 4.137; Two-way repeated measures ANOVA with Greenhouse-Geyser correction; $n = 8$ WT and $n = 9$ L7-PP2B PCs; Figure 10E).

While we have already demonstrated an impact of the strength of the complex spike response on the change in simple spike responsiveness irrespective of the clustering into strong and weak complex spike responders (Figure 9A), we further substantiated these findings in 55 WT and 23 L7-PP2B deficient PCs following separation between strong and weak responders. The correlation found between the frequency of complex spike firing and the change in simple spike activity after 4 Hz tetanic stimulation proved to be present only in the weak responders, taking the firing rate during the pre-induction and induction period into account (Figures 10 – Figure supplement 1A and B; for the diminished complex spike response during the induction period see Figure 8 – Figure supplement 1). This is again in line with the observations that parallel fiber activity in the absence of climbing fiber activity promotes parallel fiber LTP (Lev-Ram et al., 2003; Coesmans et al., 2004; Ohtsuki et al., 2009).

A comparison with the L7-PP2B mice revealed that in these mutants the relation between the complex spike frequency during the induction block and simple spike plasticity was also present (Figure 10 – Figure supplement 1C), possibly because parallel fiber LTD is probably still largely intact in these mice (Schonewille et al., 2010). Yet, in line with the absence of increased simple spike responsiveness, the correlation between changes in simple spike firing during the induction block and the impact of 4 Hz stimulation, as present in the WT PCs, was absent in the L7-PP2B mice (Figure 10 - Figure supplements 1B and 1D). Thus,

in the absence of the PP2B protein in PCs, the impact of 4 Hz tetanic stimulation on touch-evoked whisker protraction as well as on the simple spike responsiveness was strongly diminished. The correlations between complex spike and simple spike firing on the one hand and modification of the simple spike response to whisker pad stimulation on the other hand further strengthen our hypothesis that parallel fiber LTP is at least one of the main mechanisms underlying the long-term, behavioral and simple spike changes observed after 4 Hz tetanic stimulation.

Expression of AMPA receptor GluA3 subunits in Purkinje cells is required for increased protraction and simple spike firing following 4 Hz tetanic stimulation

Despite the evidence in favor of parallel fiber LTP as the underlying mechanism of the behavioral and electrophysiological impact of 4 Hz tetanic sensory stimulation, alternative explanations may exist. For instance, since PP2B is normally active in the cytoplasm of a cell, L7-PP2B mice may not only be deficient at the synaptic parallel fiber input of PCs, but also at other locations inside the cell where PP2B might serve different functions. To further investigate our hypothesis on the impact of parallel fiber LTP we used a second, independent mouse model, in which the synaptic input is more selectively affected: i.e., the L7-GluA3 deficient mice (Gutierrez-Castellanos et al., 2017). These mice lack the GluA3 subunit of the AMPA receptors specifically at their parallel fiber-to-PC synapses and consequently are less likely to have prominent cytosolic side-effects, while still having impaired parallel fiber-to-PC LTP. As in the L7-PP2B mice, we did not find evidence for increased whisker protraction after 4 Hz tetanic stimulation (e.g., change in whisker angle during the first 120 ms after air puff onset: WT vs. L7-GluA3 mice: $p = 0.007$; Tukey's post-hoc test after ANOVA ($p = 0.001$; $F = 9.111$; df = 2); $n = 16$ WT and $n = 6$ GluA3 deficient mice) (Figure 11A-C). Moreover, as in the L7-PP2B mice, also the increase in simple spike responsiveness after 4

Hz stimulation was absent in L7-GluA3 mice (simple spike count between WT and L7-GluA3 PCs during the first 60 ms after air puff onset: $p = 0.004$; Tukey's post-hoc test after ANOVA ($p = 0.002$; $F = 6.681$; df = 2); $n = 35$ WT PCs and $n = 13$ GluA3 KO PCs, next to $n = 23$ L7-PP2B KO PCs, all with weak complex spike responses) (Figure 11D-F). Thus an independent line of evidence supports the findings made in the L7-PP2B mice.

Basic PC spiking responses in L7-PP2B and L7-GluA3 mice

For control we compared the basic electrophysiological profiles of PCs in the three genotypes used in this study. When averaged over the entire period with episodes of stimulation, the overall complex spike rate, simple spike rate and simple spike CV2 value (i.e., increased regularity) of PCs in the L7-PP2B KO mice were moderately, but significantly, reduced compared to those in WTs (Figure 11 – Figure supplement 1A-D; Table S3). Likewise, the peak activity of both the complex spike responses and the simple spike responses in the periods of a few hundred ms directly following the sensory whisker stimulation were significantly reduced in the L7-PP2B KO PCs (Figure 11 – Figure supplement 1E-J; Table S3). In contrast, the L7-GluA3 KO PCs did not show any significant difference with the WT PCs as far as these parameters were concerned, except for the peak complex spike response, which was also slightly reduced compared to WT (Figure 11 – Figure supplement 1E-J; Table S3). However, as the complex spike response negatively correlates with the occurrence of behavioral and simple spike potentiation in WTs (see above), a reduced peak of the complex spike response would be more in line with an increase in potentiation and thereby an enhanced behavioral response, making it unlikely that this property could explain the phenotypes in the mutants. Thus, since the differences in basic PC spiking properties are either not consistent among the L7-PP2B and L7-GluA3 KO lines or do not show the proper polarity, the most parsimonious explanation for their common lack of behavioral and spike

learning is their virtually identically impaired levels of LTP induction (Schonewille et al., 2010; Gutierrez-Castellanos et al., 2017).

Discussion

In this study we show for the first time that touch can evoke a reflexive whisker protraction that is modifiable. As with learning of other reflexes, such as eyeblink conditioning or adaptation of the vestibulo-ocular reflex, long-term modification of this touch-evoked whisker protraction requires an intact cerebellum. We show here that a brief period of 4 Hz tetanic sensory stimulation results in enduring amplification of a touch-evoked whisker protraction. Extracellular recordings revealed that the simple spike rate of the PCs that are predominantly located laterally in *crus 2* correlates well with whisker movement and is congruently increased with enhanced whisker protraction after tetanic stimulation. These PCs show a weak complex spike response to whisker stimulation, which appears to act permissive for the occurrence of parallel fiber-to-PC LTP. This plasticity mechanism is likely to be one of the main mechanisms underlying this whisker reflex adaptation, as we found that the 4 Hz induction protocol did result neither in more whisker protraction nor in stronger simple spike responses in two independent genetic mouse models, both of which lack LTP induction at their parallel fiber-to-PC synapse. By contrast, the PCs that show a strong complex spike response to whisker stimulation and that are mainly located laterally in *crus 1* did not manifest a prominent regulatory role for their simple spike activity in long-term modification of their whisker movements. While simple spike rates were readily modifiable and had a bilateral relation with whisker movements, complex spike firing was more rigid and its coherence correlated well with the strength of the short-term touch-evoked protraction reflex itself. The whisker system is one of the first of its kind in which different modular regions of the cerebellar cortex appear to control the same motor domain with differential and complementary roles in guiding the short-term and long-term dynamics and kinematics.

Control of whisker movements

Although most mammals have whiskers, only a few species use their whiskers to actively explore their environment by making fast, rhythmic whisker movements (Welker, 1964; Woolsey et al., 1975; Ahl, 1986). In “whisking” animals, such as mice and rats, whisker protraction is under direct muscle control, while whisker retraction is largely mediated by a passive process involving skin elasticity (Berg and Kleinfeld, 2003; Simony et al., 2010; Haidarliu et al., 2015). Animals can modify the pattern of whisker movements upon sensory feedback during natural behavior, as has been demonstrated for example during gap crossing and prey capture (Anjum and Brecht, 2012; Voigts et al., 2015). The neural control of reflexive whisker movements and adaptation thereof is still largely unknown. We show here, at least for a specific reproducible form of whisker adaptation, that this is under control of the cerebellum.

Complex spike activity in relation to reflexive whisker movements

The functional role of complex spike responses is still under debate. Whereas some advocate a primary role as a dynamic metronome driving motor timing (Lang et al., 1999; Yamamoto et al., 2001; Llinás, 2011), others claim a more indirect role as a teacher guiding motor learning through sensory error signals (Ito, 2001; Yang and Lisberger, 2014; Herzfeld et al., 2018), or a combination of these short-time and long-term functions (Van Der Giessen et al., 2008; Mathy et al., 2009; Ten Brinke et al., 2015). The whisker stimulation in our paradigm resulted in strong complex spike responses particularly in the lateral PCs of *crus 1*. Even though the complex spikes were present only in a minority of the trials of individual PCs, the complex spike responses typically occurred simultaneously in many PCs, highlighting a putative role for ensemble encoding (Mukamel et al., 2009; Ozden et al., 2009; Schultz et al., 2009; Hoogland et al., 2015). Indeed, not only did the complex spike responses increase prior

to whisker protraction, but the coherent firing of these complex spikes also proved to be correlated with increased protraction (Figures 4 and 5), which is in line with previous studies showing that complex spikes can facilitate the initiation of movements and define their amplitude (Welsh et al., 1995; Kitazawa et al., 1998; Hoogland et al., 2015). Possibly, the complex spikes of the PCs on one side of the cerebellum also contribute to the whisker movements on the contralateral side via bilateral projections of the cerebellar nuclei to the reticular formation (Teune et al., 2000), because stimulating the contralateral whisker pad also resulted in a strong protraction, while the complex spikes on the ipsilateral side were much less responsive during contralateral stimulation (Figure 7). The level of complex spike firing was correlated to the level of whisker retraction induced by the initial air flow, which agrees with the notion that complex spikes often signal the mismatch between the actual and expected sensory input (Gilbert and Thach, 1977; Gellman et al., 1983; Graf et al., 1988; Stone and Lisberger, 1990). Hence, complex spikes of the whisker regions in the cerebellar cortex are associated with both sensory responses and the generation of motor output.

Simple spike firing during normal and adapted whisker movements

Our electrophysiological recordings indicate that the simple spike activity of many PCs in *crus 2* correlates well with whisker protraction and that this relation is context-dependent. Under the baseline condition of our paradigm, during the 0.5 Hz whisker pad stimulation, the simple spikes correlate on single trial basis well with the position of the whiskers during protraction. The correlation between more simple spikes and more protraction was also found when comparing the impact of contralateral vs. ipsilateral whisker pad stimulation. The absence of a clear time lag or lead between the simple spike activity and the whisker movements under this condition suggests that during normal motor performance without sensorimotor mismatch signaling the simple spikes represent the ongoing movement. Our data

under baseline conditions are also compatible with those obtained by the labs of Chadderton and Léna (Proville et al., 2014; Chen et al., 2016). In their studies on online motor performance, the simple spike activity of most PCs in the lateral *crus 1* and/or *crus 2* regions correlated best with protraction of the set point, defined as the slowly varying midpoint between maximal protraction and maximal retraction. This relation was, as in our study, state-dependent in that the general level of movement activity had a strong impact on the correlation between simple spike firing and whisker movement. However, our data revealed that under the training condition, during and directly after the 4 Hz tetanic stimulation protocol, the temporal dynamics of the simple spikes shifted. As a result, the best correlation between simple spikes and whisker position was now found to precede the whisker movement and to predict the magnitude of the protraction, suggesting an instructive motor function for the simple spikes during learning. Thus, the current dataset confirms and expands on previous studies, highlighting a role of the cerebellar PCs injecting additional accelerating and amplifying signals into the cerebellar nuclei during entrainment.

Cerebellar plasticity

Synaptic plasticity in the cerebellar cortex has, next to that in the cerebellar and vestibular nuclei (Lisberger and Miles, 1980; Lisberger, 1998), generally been recognized as one of the major mechanisms underlying motor learning (Ito, 2001, 2003). Most attention has been directed towards LTD of the parallel fiber-to-PC synapse (Albus, 1971; Ito, 2003; Linden, 2003). Indeed, sparsification of simple spike firing happens during eyeblink conditioning (Jirenhed et al., 2007; Ten Brinke et al., 2015), while trial-over-trial suppression of simple spike firing occurs during smooth pursuit training (Yang and Lisberger, 2014; Herzfeld et al., 2018). In recent years, other forms of synaptic plasticity have also attracted attention, calling into question whether parallel fiber LTD is the only dominant mechanism in the cerebellar

cortex underlying learning. Several forms of procedural learning, such as adaptation of the vestibulo-ocular reflex, turned out to be impaired in various genetic mouse models deficient in parallel fiber-to-PC LTP (Schonewille et al., 2010; Ly et al., 2013; Rahmati et al., 2014; Peter et al., 2016; Gutierrez-Castellanos et al., 2017). These findings were corroborated using optogenetic stimulation of PCs in the vestibulocerebellum so as to increase the gain of the vestibulo-ocular reflex (Voges et al., 2017). Cerebellar plasticity may therefore be more heterogeneous than previously thought (Hansel et al., 2001; Gao et al., 2012; D'Angelo et al., 2016). The dominant form of plasticity in the cerebellar cortex may vary dependent on the zebrin-expression pattern of the PC module involved (De Zeeuw and Ten Brinke, 2015). PCs in zebrin-positive modules, which have a relatively low baseline simple spike firing rate with ample room for increases, may be more prone for induction of potentiation, whereas the zebrin-negative zones, which have a relatively high baseline firing rate, may tend to engage various forms of plasticity that promote simple spike suppression (Zhou et al., 2014; De Zeeuw and Ten Brinke, 2015). The area in which we found the strongest correlation between simple spike firing and whisker position is largely zebrin-positive, predominantly corresponding to the 6+ and 7+ zones (Sugihara and Quy, 2007). Accordingly, most PCs in our study had a relatively low baseline simple spike frequency (Figure 11 – Figure supplement 1C) and two independent mouse models lacking parallel fiber LTP specifically in their PCs (i.e., the L7-PP2B and L7-GluA3 mice) manifested robust impairments in adaptation of whisker protraction. In addition, the PCs that were engaged in adaptation of whisker protraction did not only show an increase in their simple spike response, but they also showed only a weak complex spike response during the training stimuli, which is indeed permissive for the induction of parallel fiber-to-PC LTP (Coesmans et al., 2004). Thus, our study is one of the first to show a direct coupling between an increase in simple spike firing

and motor learning, with both phenomena being absent in independent mouse models lacking parallel fiber LTP.

In conclusion

Whisker protraction can be elicited as a reflex following mechanical manipulation and the short-term kinematics of this reflex appears to be at least partly facilitated by coherent complex spike activity of PCs in the lateral part of *crus 1*. The long-term kinematics of the reflex can be adapted by tetanic stimulation and this process is probably largely mediated by increases in simple spike activity of PCs in the lateral part of *crus 2*, which may have been facilitated by the induction of LTP at their parallel fiber inputs. The differentially distributed, short-term and long-term cerebellum-dependent modulation of whisker movements may well play a role in motor coordination and adaptation during performance and acquisition of whisking behaviors like gap crossing and prey capture, which probably require both fast reflexes and long-term skills (Anjum and Brecht, 2012; Voigts et al., 2015). When compared to other motor behaviors controlled by other zebrin-positive regions, such as adaptation of the vestibulo-ocular reflex around different axes in space controlled by different modules in the flocculus of the vestibulocerebellum (Simpson et al., 1996; Ito, 2003; De Zeeuw and Ten Brinke, 2015), the whisker system appears to be rather unique in that it is the first of its kind in which different modular regions of the cerebellar cortex appear to control the same motor domain with complementary roles in differentially guiding the short-term and long-term dynamics of the movement involved.

Acknowledgements

Financial support was provided by the Netherlands Organization for Scientific Research (NWO-ALW; C.I.D.Z.), the Dutch Organization for Medical Sciences (ZonMW; C.I.D.Z.), Life Sciences (C.I.D.Z.), ERC-adv and ERC-POC (C.I.D.Z.) and the China Scholarship Council (No. 2010623033; C.J.). We thank E. Haasdijk, E. Goedknegt, M. Rutteman, and A.C.H.G. IJpelaar for technical assistance and Drs. T. Ruigrok, S. Koekkoek, and M. Schonewille of the Neuroscience Department at the Erasmus Medical Center for their input and scientific discussions, as well as Dr. D. Rizopoulos of the Biostatistics Department at the Erasmus Medical Center and Dr. D. Vidotto from Tilburg University for statistical consulting regarding the cluster analysis.

Competing financial interests

The authors declare no competing financial interests.

Methods

Animals

In this study, we used two different mutant mouse lines, both on a C57Bl/6J background. Comparisons of electophysiological parameters were always made between the mutant mice and their respective wild-type (WT) littermates, although for easier visualization the WTs were sometimes grouped as indicated in the figure legends. Both mouse lines had been used before and details on their generation have been published. Briefly, L7-PP2B mice (Tg(Pcp2-cre)2MPin;Ppp3r1^{tm1Stl}) lacked functional PP2B specifically in their Purkinje cells (PCs). They were created by crossing mice in which the gene for the regulatory subunit (CNB1) of PP2B was flanked by loxP sites (Zeng et al., 2001) with transgenic mice expressing Cre-recombinase under control of the L7 (Pcp2) promoter (Barski et al., 2000) as described in Schonewille et al. (2010). L7-Cre$^{+/-}$-cnb1$^{f/f}$ mice ("L7-PP2B mice") were compared with L7-Cre$^{-/-}$-cnb1$^{f/f}$ littermate controls. We used 35 WT mice (17 males and 18 females of 21 ± 9 weeks of age (average ± s.d.)) and 22 L7-PP2B mice (6 males and 16 females of 18 ± 10 weeks of age (average ± s.d.)). L7-GluA3 mice (Tg(Pcp2-cre)2MPin;Gria3^{tm2Rsp}) lacked the AMPA receptor GluA3 subunit specifically in their PCs. They were created by crossing mice in which the *Gria3* gene was flanked by loxP sites (Sanchis-Segura et al., 2006) with transgenic mice expressing Cre-recombinase under control of the L7 (Pcp2) promoter (Barski et al., 2000) as described in Gutierrez-Castellanos et al. (2017). We used L7-Cre$^{+/-}$-Gria3$^{f/f}$ mice ("L7-GluA3 mice") and L7-Cre$^{-/-}$-Gria3$^{f/f}$ as littermate controls. We used 5 WT male mice (25 ± 3 weeks of age (average ± s.d.)) and 9 L7-GluA3 mice (6 males and 3 females of 26 ± 4 weeks of age (average ± s.d.)). Mutants and wild-types were measured in random sequence. For the two-photon Ca^{2+} imaging experiments, we used 6 male C57Bl/6J mice (Charles Rivers, Leiden, the Netherlands) of 4-12 weeks of age. The photostimulation experiments were performed on 7 mice (3 males and 4 females of 25 ± 1 weeks of age

(average ± s.d.)) expressing Channelrhodopsin-2 exclusively in their PCs (Tg(Pcp2-cre)2MPin;Gt(ROSA)26Sor$^{tm27.1(CAG-COP4*H134R/tdTomato)Hze}$) as described previously (Witter et al., 2013). The lack of impact of gender on key parameters of this study was documented in Table S4. All mice were socially housed until surgery and single-housed afterwards. The mice were kept at a 12/12 h light/dark cycle and had not been used for any invasive procedure (except genotyping shortly after birth) before the start of the experiment. All mice used were specific-pathogen free (SPF). All experimental procedures were approved a priori by an independent animal ethical committee (DEC-Consult, Soest, The Netherlands) as required by Dutch law and conform the relevant institutional regulations of the Erasmus MC and Dutch legislation on animal experimentation.

Surgery

All mice that were used for electrophysiology received a magnetic pedestal that was attached to the skull above bregma using Optibond adhesive (Kerr Corporation, Orange, CA) and a craniotomy was made on top of crus 1 and crus 2. The surgical procedures were performed under isoflurane anesthesia (2-4% V/V in O_2). Post-surgical pain was treated with 5 mg/kg carprofen ("Rimadyl", Pfizer, New York, NY, USA), 1 µg lidocaine (Braun, Meisingen, Germany), 1 µg bupivacaine (Actavis, Parsippany-Troy Hills, NJ, USA) and 50 µg/kg buprenorphine ("Temgesic", Indivior, Richmond, VA, USA). After three days of recovery, mice were habituated to the recording setup during at least 2 daily sessions of approximately 45 min. In the recording setup they were head-fixed using the magnetic pedestal. The mice used for two-photon imaging received a head plate with a sparing on the location of the craniotomy instead of a pedestal. The head plate was attached to the skull with dental cement (Superbond C&B, Sun Medical Co., Moriyama City, Japan). To prevent the growth of scar

tissue, which could affect image quality, two-photon recordings were made on the day of the surgery (recording started at least 1 h after the termination of anesthesia).

Whisker stimulation and tracking

Air puff stimulation to the whisker pad was applied with a frequency of 0.5 Hz s at a distance of approximately 3 mm at an angle of approximately 35° (relative to the body axis). The puffs were delivered using a tube with a diameter of approximately 1 mm with a pressure of ~2 bar and a duration of 30 ms. During the induction period, the stimulation frequency was increased to 4 Hz and 80 puffs were given. In a subset of experiments, a 2 ms air puff (pre-pulse) was delivered 100 ms prior to the 30 ms puff. Videos of the whiskers were made from above using a bright LED panel as backlight (λ = 640 nm) at a frame rate of 1,000 Hz (480x500 pixels using an A504k camera from Basler Vision Technologies, Ahrensburg, Germany). The whiskers were not trimmed or cut.

Electrophysiology

Electrophysiological recordings were performed in awake L7-PP2B WT mice using either glass pipettes (3-6 MΩ) or quartz-coated platinum/tungsten electrodes (2-5 MΩ, outer diameter = 80 µm, Thomas Recording, Giessen, Germany). The latter electrodes were placed in an 8x4 matrix (Thomas Recording), with an inter-electrode distance of 305 µm. Prior to the recordings, the mice were lightly anesthetized with isoflurane to remove the dura, bring them in the setup and adjust all manipulators. Recordings started at least 60 min after termination of anesthesia and were made in crus 1 and crus 2 ipsilateral to the side of the whisker pad stimulation at a minimal depth of 500 µm. The electrophysiological signal was digitized at 25 kHz, using a 1-6,000 Hz band-pass filter, 22x pre-amplified and stored using a RZ2 multi-channel workstation (Tucker-Davis Technologies, Alachua, FL).

Neural tracing & electrolytic lesions

For the neural tracing experiments, we used glass electrodes filled with 2 M NaCl for juxtacellular recordings. After a successful recording of a PC, neural tracer was pressure injected (3 x 10 ms with a pressure of 0.7 bar) either from the same pipette re-inserted at the same location or from the second barrel or a double barrel pipette. We used a gold-lectin conjugate has described previously (Ruigrok et al., 1995) (n = 3) or biotinylated dextran amine (BDA) 3000 (10 mg/ml in 0.9% NaCl; ThermoFisher Scientific, Waltham, MA, USA) (n = 7). Five days after the tracer injection, the mice were anesthetized with pentobarbital (80 mg/kg intraperitoneal) and fixated by transcardial perfusion with 4% paraformaldehyde. The brains were removed and sliced (40 µm thick). The slices were processed by Nissl staining. Experiments were included in the analysis if the electrophysiology fulfilled the requirements mentioned above with a recording duration of at least 50 s and if the tracer was clearly visible. For BDA 3000 this implied that it was taken up by the PCs at the injection spot and transported to the axonal boutons a single subgroup in the cerebellar nuclei. BDA 3000 was also found in the inferior olive. For the gold-lectin conjugate the subnucleus of the inferior olive was considered. Based upon the subnuclei of the cerebellar nuclei and/or the inferior olive, the sagittal zone of the recording site was identified according to the scheme published in Apps and Hawkes (2009).

After the recordings made with the quartz/platinum electrodes, electrolytic lesions were applied to selected electrodes in order to retrieve the recording locations. To this end, we applied a DC current of 20 µA for 20 s. This typically resulted in a lesion that could be visualized after Nissl staining of 40 µm thick slices made of perfused brains. We accepted a spot as a true lesion if it was visible in at least 2 consecutive slices at the same location. In

total, we could retrieve 16 successful lesions. Recording locations were approximated using pictures of the entry points of the electrodes in combination with the locations of the lesions.

Two-photon Ca^{2+} imaging

After the surgery (see above) with the dura mater intact, the surface of the cerebellar cortex was rinsed with extracellular solution composed of (in mM) 150 NaCl, 2.5 KCl, 2 $CaCl_2$, 1 $MgCl_2$ and 10 HEPES (pH 7.4, adjusted with NaOH). After a 30 minute recovery period from anesthesia animals were head-fixed in the recording setup and received a bolus-loading of the cell-permeant fluorescent Ca^{2+} indicator Cal-520 AM (0.2 mM; AAT Bioquest, Sunnyvale, CA, USA). The dye was first dissolved with 10% w/V Pluronic F-127 in DMSO (Invitrogen) and diluted 20x in the extracellular solution. The dye solution was pressure injected into the molecular layer (50–80 µm below the surface) at 0.35 bar for 5 min. After dye loading, the brain surface was covered with 2% agarose dissolved in saline (0.9% NaCl) in order to reduce motion artefacts and prevent dehydration.

Starting at least 30 min after dye injection, *in vivo* two-photon Ca^{2+} imaging was performed of the molecular layer using a setup consisting of a titanium sapphire laser (Chameleon Ultra, Coherent, Santa Clara, CA), a TriM Scope II system (LaVisionBioTec, Bielefeld, Germany) mounted on a BX51 microscope with a 20x 1.0 NA water immersion objective (Olympus, Tokyo, Japan) and GaAsP photomultiplier detectors (Hamamatsu, Iwata City, Japan). A typical recording sampled 40 x 200 µm with a frame rate of approximately 25 Hz.

Data inclusion

We included all mice measured during this study, with the exception of one mouse where video-analysis revealed that the air puff was delivered more to the nose than to the whisker

pad. Single-unit data was included if the recording was of sufficient quality and reflected the activity of a single PC according to the rules defined below (see section *Electrophysiological analysis*).

Whisker tracking

Whisker movements were tracked offline as described previously (Rahmati et al., 2014) using a method based on the BIOTACT Whisker Tracking Tool (Perkon et al., 2011). We used the average angle of all trackable large facial whiskers for further quantification of whisker behavior.

The impact of 4 Hz tetanic stimulation on air puff-triggered whisker movement was quantified using a bootstrap method. First, we took the last 100 trials before induction and divided these randomly in two series of 50. We calculated the differences in whisker position between these two series, and repeated this 1000 times. From this distribution we derived the expected variation after whisker pad air puff stimulation. We took the 99% confidence interval as the threshold to which we compared the difference between 50 randomly chosen trials after and 50 randomly chosen trials before induction (Figure 10C).

Electrophysiological analysis

Spikes were detected offline using SpikeTrain (Neurasmus, Rotterdam, The Netherlands). A recording was considered to originate from a single PC when it contained both complex spikes (identified by the presence of stereotypic spikelets) and simple spikes, when the minimal inter-spike interval of simple spikes was 3 ms and when each complex spike was followed by a pause in simple spike firing of at least 8 ms. The regularity of simple spike firing was expressed as the local variation (CV2) and calculated as $2|ISI_{n+1}-ISI_n|/(ISI_{n+1}+ISI_n)$ with ISI = inter-simple spike interval (Shin et al., 2007). Only single-unit recordings of PCs

with a minimum recording duration of 200 s were selected for further analysis. However, for the neural tracing experiments (see below), on which no quantitative analysis was performed, we accepted a minimum recording duration of 50 s.

Two-photon Ca^{2+} imaging analysis

Image analysis was performed offline using custom made software as described and validated previously (Ozden et al., 2012; De Gruijl et al., 2014). In short, we performed independent component analysis to define the areas of individual Purkinje cell dendrites (Figure 4A). The fluorescent values of all pixels in each region of interest were averaged per frame. These averages were plotted over time using a high-pass filter. A 8% rolling baseline was subtracted with a time window of 0.5 ms (Ozden et al., 2012). Ca^{2+} transients were detected using template matching.

For the aggregate peri-stimulus time histograms (PSTHs) (Figure 4D), we calculated per individual frame the number of complex spikes detected and made a PSTH color coding the number of simultaneously detected complex spikes. Based upon the total number of complex spikes and dendrites per recording, we calculated the expected number of simultaneous complex spikes per individual frame based upon a Poisson distribution. The actual number of simultaneous complex spikes was compared to this calculated distribution and a *p* value was derived for each number based upon the Poisson distribution (Figure 4E).

Characterization of sensory responses

For each PC recording, we constructed PSTHs of complex spikes and simple spikes separately using a bin size of 10 ms for display purposes. For further quantitative analyses of the PSTHs, we used a bin size of 1 ms and convolved them with a 21 ms wide Gaussian kernel. Complex spike responses were characterized by their peak amplitude, defined as the

maximum of the convolved PSTH and expressed in percentage of trials in which a complex spike occurred within a 1 ms bin. Latencies were taken as the time between stimulus onset and the time of the response peak, as determined from the convolved PSTH.

For some analyses, we discriminated between the sensory response period (0-60 ms after stimulus onset) and inter-trial interval (500 to 200 ms before stimulus onset). We considered a PC responsive for sensory stimulation if the peak or trough in the PSTH in the 60 ms after the stimulus onset exceeded the threshold of 3 s.d. above or below the average of the pre-stimulus interval (1 ms bins convolved with a 21 ms Gaussian kernel, pre-stimulus interval 200 ms before stimulus onset).

Long-term stability of electrophysiological recordings was verified by heat maps of time-shifted PSTHs (e.g., see Figures 9E and 11E). The time-shifted PSTH was processed by calculating the simple spike PSTH for 20 air puffs per row, which were shifted by 5 air puffs between neighboring rows. The simple spike rates per row are calculated at 1 ms resolution and convolved with a 21 ms Gaussian kernel and color-coded relative to baseline firing rate (-1000 to -200 ms relative to air puff time).

Cluster analysis

A principal component analysis showed that the heterogeneity among the sensory complex spike responses was driven almost exclusively by one parameter, the maximum amplitude peak of the convolved complex spike PSTH. We performed a univariate Gaussian mixture model using only that variable. The Bayesian information criterion (BIC) indicated that the model with two components with unequal variances yielded the best approximation of the data. Then we applied the function Mclust(data) in R (R Foundation, Vienna, Austria) which use the expectation-maximization algorithm in order to assert the main parameters of the resulting models (probability, mean and variance of each population).

Spikes-whisker movement correlation matrix

Trial-by-trial correlation between instantaneous simple spike firing rate and whisker position was performed as described before (Ten Brinke et al., 2015). In short: spike density functions were computed for all trials by convolving spike occurrences across 1 ms bins with an 8 ms Gaussian kernel. Both spike and whisker data were aligned to the 200 ms baseline. For cell groups, data was standardized for each cell for each correlation, and then pooled. The spike-whisker Pearson correlation coefficient R was calculated in bin of 10 ms, resulting in a 40x40 R-value matrix showing correlations for -100 to 300 ms around the air puff presentation.

Statistical analysis

Group sizes of the blindly acquired data sets were not defined a priori as the effect size and variation were not known beforehand. A post hoc power calculation based upon the results of the potentiation of the PC responses to whisker pad stimulation of the "weak complex spike responders" indicated a minimum group size of 12 PCs (α = 5%, β = 20%, Δ = 9.65%, s.d. = 10.59%, paired *t* test). This number was obtained for the "weak complex spike responders" in WT (n = 35), L7-PP2B (n = 21) and L7-GluA3 PCs (n = 13), as well as for the relatively rare "strong complex spike responders" in WT mice (n = 20). This was further substantiated by other independent analyses, including ANOVA and linear regression, as described in the Results section. Variations in success rate, especially considering recordings of longer duration in combination with video tracking, explain why some groups are larger than others. Data was excluded only in case of a signal to noise ratio that was insufficient to warrant reliable analysis. For data visualization and statistical analysis, we counted the number of PCs as the number of replicates for the spike-based analyses and the number of mice for the behavior-based analyses.

We tested whether the observed increase in coherence after sensory stimulation (Figure 4D-G) was more than expected from the increased firing rate induced by the stimulation. The expected coherence based on the firing rate was calculated from 1000 bootstrapped traces from the inhomogeneous Poisson spike trains made for each neuron. The resultant distribution was compared to the measured distribution using a two-sample Kolmogorov-Smirnov test.

Stacked line plots were generated by cumulating the values of all subjects per time point. Thus, the first line (darkest color) represents the first subject, the second line the sum of the first two, the third line the first three, etcetera. The data are divided by the number of subjects, so that the last line (brightest color) represents, next to the increase from the one but last value, also the population average.

Sample size and measures for mean and variation are specified throughout the text and figure legends. For normally distributed data (as evaluated using the Kolmogorov-Smirnov test) parametric tests were used. Comparisons were always made with 2-sided tests when applicable. Unpaired *t* test were always made with Welch correction for possible differences in s.d..

Data and software availability

All relevant data is available from the authors. Custom written Matlab code to complement the whisker tracking analysis by the BIOTACT Whisker Tracking Tool was used as described previously (Rahmati et al., 2014) and can be obtained from the authors.

References

Ahl AS (1986) The role of vibrissae in behavior: a status review. Vet Res Commun 10:245-268, doi:10.1007/BF02213989.

Alba A, Kano M, Chen C, Stanton ME, Fox GD, Herrup K, Zwingman TA, Tonegawa S (1994) Deficient cerebellar long-term depression and impaired motor learning in mGluR1 mutant mice. Cell 79:377-388, doi:10.1016/0092-8674(94)90205-4.

Albus JS (1971) Theory of cerebellar function. Math Biosci 10:25-61, doi:10.1016/0025-5564(71)90051-4.

Anjum F, Brecht M (2012) Tactile experience shapes prey-capture behavior in Etruscan shrews. Front Behav Neurosci 6:28, doi:10.3389/fnbeh.2012.00028.

Apps R, Hawkes R (2009) Cerebellar cortical organization: a one-map hypothesis. Nat Rev Neurosci 10:670-681, doi:10.1038/nrn2698.

Arkley K, Tiktak GP, Breakell V, Prescott TJ, Grant RA (2017) Whisker touch guides canopy exploration in a nocturnal, arboreal rodent, the Hazel dormouse (*Muscardinus avellanarius*). J Comp Physiol A Neuroethol Sens Neural Behav Physiol 203:133-142, doi:10.1007/s00359-017-1146-z.

Badura A, Schonewille M, Voges K, Galliano E, Renier N, Gao Z, Witter L, Hoebeek FE, Chedotal A, De Zeeuw CI (2013) Climbing fiber input shapes reciprocity of Purkinje cell firing. Neuron 78:700-713, doi:10.1016/j.neuron.2013.03.018.

Barski JJ, Dethleffsen K, Meyer M (2000) Cre recombinase expression in cerebellar Purkinje cells. Genesis 28:93-98, doi:10.1002/1526-968X(200011/12)28:3/4<93::AID-GENE10>3.0.CO;2-W.

Berg RW, Kleinfeld D (2003) Rhythmic whisking by rat: retraction as well as protraction of the vibrissae is under active muscular control. J Neurophysiol 89:104-117, doi:10.1152/jn.00600.2002.

Bosman LWJ, Koekkoek SKE, Shapiro J, Rijken BFM, Zandstra F, van der Ende B, Owens CB, Potters JW, de Gruijl JR, Ruigrok TJH, De Zeeuw CI (2010) Encoding of whisker input by cerebellar Purkinje cells. J Physiol 588:3757-3783, doi:10.1113/jphysiol.2010.195180.

Bosman LWJ, Houweling AR, Owens CB, Tanke N, Shevchouk OT, Rahmati N, Teunissen WHT, Ju C, Gong W, Koekkoek SKE, De Zeeuw CI (2011) Anatomical pathways involved in generating and sensing rhythmic whisker movements. Front Integr Neurosci 5:53, doi:10.3389/fnint.2011.00053.

Brecht M (2007) Barrel cortex and whisker-mediated behaviors. Curr Opin Neurobiol 17:408-416, doi:10.1016/j.conb.2007.07.008.

Brooks JX, Carriot J, Cullen KE (2015) Learning to expect the unexpected: rapid updating in primate cerebellum during voluntary self-motion. Nat Neurosci 18:1310-1317, doi:10.1038/nn.4077.

Brown IE, Bower JM (2001) Congruence of mossy fiber and climbing fiber tactile projections in the lateral hemispheres of the rat cerebellum. J Comp Neurol 429:59-70, doi:10.1002/1096-9861(20000101)429:1<59::AID-CNE5>3.0.CO;2-3 [pii].

Catz N, Dicke PW, Thier P (2008) Cerebellar-dependent motor learning is based on pruning a Purkinje cell population response. Proc Natl Acad Sci U S A 105:7309-7314, doi:10.1073/pnas.0706032105.

Chen S, Augustine GJ, Chadderton P (2016) The cerebellum linearly encodes whisker position during voluntary movement. Elife 5, doi:10.7554/eLife.10509.

Chen S, Augustine GJ, Chadderton P (2017) Serial processing of kinematic signals by cerebellar circuitry during voluntary whisking. Nat Commun 8:232, doi:10.1038/s41467-017-00312-1.

Christian KM, Thompson RF (2003) Neural substrates of eyeblink conditioning: acquisition and retention. Learn Mem 10:427-455, doi:10.1101/lm.59603.

Chu CP, Bing YH, Qiu DL (2011) Sensory stimulus evokes inhibition rather than excitation in cerebellar Purkinje cells *in vivo* in mice. Neurosci Lett 487:182-186, doi:10.1016/j.neulet.2010.10.018.

880 Coesmans M, Weber JT, De Zeeuw CI, Hansel C (2004) Bidirectional parallel fiber plasticity in the
881 cerebellum under climbing fiber control. Neuron 44:691-700,
882 doi:10.1016/j.neuron.2004.10.031.
883 D'Angelo E, Nieus T, Maffei A, Armano S, Rossi P, Taglietti V, Fontana A, Naldi G (2001) Theta-
884 frequency bursting and resonance in cerebellar granule cells: experimental evidence and
885 modeling of a slow k+-dependent mechanism. J Neurosci 21:759-770,
886 doi:10.1523/JNEUROSCI.21-03-00759.2001.
887 D'Angelo E, Mapelli L, Casellato C, Garrido JA, Luque N, Monaco J, Prestori F, Pedrocchi A, Ros E
888 (2016) Distributed circuit plasticity: new clues for the cerebellar mechanisms of learning.
889 Cerebellum 15:139-151, doi:10.1007/s12311-015-0711-7.
890 De Gruijl JR, Hoogland TM, De Zeeuw CI (2014) Behavioral correlates of complex spike synchrony in
891 cerebellar microzones. J Neurosci 34:8937-8944, doi:10.1523/JNEUROSCI.5064-13.2014.
892 De Zeeuw CI, Ten Brinke MM (2015) Motor learning and the cerebellum. Cold Spring Harb Perspect
893 Biol 7:a021683, doi:10.1101/cshperspect.a021683.
894 De Zeeuw CI, Hoebeek FE, Bosman LWJ, Schonewille M, Witter L, Koekkoek SK (2011) Spatiotemporal
895 firing patterns in the cerebellum. Nat Rev Neurosci 12:327-344, doi:10.1038/nrn3011.
896 Dehnhardt G, Mauck B, Hanke W, Bleckmann H (2001) Hydrodynamic trail-following in harbor seals
897 (*Phoca vitulina*). Science 293:102-104, doi:10.1126/science.1060514.
898 Dere E, Huston JP, De Souza Silva MA (2007) The pharmacology, neuroanatomy and neurogenetics of
899 one-trial object recognition in rodents. Neurosci Biobehav Rev 31:673-704,
900 doi:10.1016/j.neubiorev.2007.01.005.
901 Deschênes M, Kurnikova A, Elbaz M, Kleinfeld D (2016) Circuits in the ventral medulla that phase-lock
902 motoneurons for coordinated sniffing and whisking. Neural Plast 2016:7493048,
903 doi:10.1155/2016/7493048.
904 Diamond ME, Arabzadeh E (2013) Whisker sensory system - From receptor to decision. Progress in
905 Neurobiology 103:284-240, doi:10.1016/j.pneurobio.2012.05.013.
906 Feldmeyer D, Brecht M, Helmchen F, Petersen CCH, Poulet JFA, Staiger JF, Luhmann HJ, Schwarz C
907 (2013) Barrel cortex function. Progress in Neurobiology 103:3-27,
908 doi:10.1016/j.pneurobio.2012.11.002.
909 Ferezou I, Haiss F, Gentet LJ, Aronoff R, Weber B, Petersen CCH (2007) Spatiotemporal dynamics of
910 cortical sensorimotor integration in behaving mice. Neuron 56:907-923.,
911 doi:10.1016/j.neuron.2007.10.007.
912 Gao Z, Van Beugen BJ, De Zeeuw CI (2012) Distributed synergistic plasticity and cerebellar learning.
913 Nat Rev Neurosci 13:619-635, doi:10.1038/nrn3312.
914 Gellman R, Houk JC, Gibson AR (1983) Somatosensory properties of the inferior olive of the cat. J
915 Comp Neurol 215:228-243, doi:10.1002/cne.902150210.
916 Gilbert PF, Thach WT (1977) Purkinje cell activity during motor learning. Brain Res 128:309-328,
917 doi:10.1016/0006-8993(77)90997-0.
918 Gogan P (1970) The startle and orienting reactions in man. A study of their characteristics and
919 habituation. Brain Res 18:117-135, doi:10.1016/0006-8993(70)90460-9.
920 Graf W, Simpson JI, Leonard CS (1988) Spatial organization of visual messages of the rabbit's
921 cerebellar flocculus. II. Complex and simple spike responses of Purkinje cells. J Neurophysiol
922 60:2091-2121, doi:10.1152/jn.1988.60.6.2091.
923 Guo ZV, Li N, Huber D, Ophir E, Gutnisky D, Ting JT, Feng G, Svoboda K (2014) Flow of cortical activity
924 underlying a tactile decision in mice. Neuron 81:179-194, doi:10.1016/j.neuron.2013.10.020.
925 Gutierrez-Castellanos N, Da Silva-Matos CM, Zhou K, Canto CB, Renner MC, Koene LMC, Ozyildirim O,
926 Sprengel R, Kessels HW, De Zeeuw CI (2017) Motor learning requires Purkinje cell synaptic
927 potentiation through activation of AMPA-receptor subunit GluA3. Neuron 93:409-424,
928 doi:10.1016/j.neuron.2016.11.046.
929 Haidarliu S, Kleinfeld D, Deschênes M, Ahissar E (2015) The musculature that drives active touch by
930 vibrissae and nose in mice. Anat Rec (Hoboken) 298:1347-1358, doi:10.1002/ar.23102.

Hansel C, Linden DJ, D'Angelo E (2001) Beyond parallel fiber LTD: the diversity of synaptic and non-synaptic plasticity in the cerebellum. Nat Neurosci 4:467-475, doi:10.1038/87419.

Heiney SA, Wohl MP, Chettih SN, Ruffolo LI, Medina JF (2014) Cerebellar-dependent expression of motor learning during eyeblink conditioning in head-fixed mice. J Neurosci 34:14845-14853, doi:10.1523/JNEUROSCI.2820-14.2014.

Herzfeld DJ, Vaswani PA, Marko MK, Shadmehr R (2014) A memory of errors in sensorimotor learning. Science 345:1349-1353, doi:10.1126/science.1253138.

Herzfeld DJ, Kojima Y, Soetedjo R, Shadmehr R (2015) Encoding of action by the Purkinje cells of the cerebellum. Nature 526:439-442, doi:10.1038/nature15693.

Herzfeld DJ, Kojima Y, Soetedjo R, Shadmehr R (2018) Encoding of error and learning to correct that error by the Purkinje cells of the cerebellum. Nat Neurosci 21:736-743, doi:10.1038/s41593-018-0136-y.

Hoogland TM, De Gruijl JR, Witter L, Canto CB, De Zeeuw CI (2015) Role of synchronous activation of cerebellar Purkinje cell ensembles in multi-joint movement control. Curr Biol 25:1157-1165, doi:10.1016/j.cub.2015.03.009.

Ito M (2001) Cerebellar long-term depression: characterization, signal transduction, and functional roles. Physiol Rev 81:1143-1195., doi:10.1152/physrev.2001.81.3.1143.

Ito M (2003) Long-term depression. Annu Rev Neurosci 12:85-102, doi:10.1146/annurev.ne.12.030189.000505.

Jirenhed DA, Bengtsson F, Hesslow G (2007) Acquisition, extinction, and reacquisition of a cerebellar cortical memory trace. J Neurosci 27:2493-2502, doi:10.1523/JNEUROSCI.4202-06.2007.

Kitazawa S, Kimura T, Yin PB (1998) Cerebellar complex spikes encode both destinations and errors in arm movements. Nature 392:494-497, doi:10.1038/33141.

Kleinfeld D, Berg RW, O'Connor SM (1999) Anatomical loops and their electrical dynamics in relation to whisking by rat. Somatosens Mot Res 16:69-88,

Koekkoek SKE, Hulscher HC, Dortland BR, Hensbroek RA, Elgersma Y, Ruigrok TJH, De Zeeuw CI (2003) Cerebellar LTD and learning-dependent timing of conditioned eyelid responses. Science 301:1736-1739, doi:10.1126/science.1088383.

Konnerth A, Dreessen J, Augustine GJ (1992) Brief dendritic calcium signals initiate long-lasting synaptic depression in cerebellar Purkinje cells. Proc Natl Acad Sci U S A 89:7051-7055., doi:10.1073/pnas.89.15.7051.

Lang EJ, Sugihara I, Welsh JP, Llinás R (1999) Patterns of spontaneous purkinje cell complex spike activity in the awake rat. J Neurosci 19:2728-2739, doi:10.1523/JNEUROSCI.19-07-02728.1999

Lev-Ram V, Wong ST, Storm DR, Tsien RY (2002) A new form of cerebellar long-term potentiation is postsynaptic and depends on nitric oxide but not cAMP. Proc Natl Acad Sci U S A 99:8389-8393., doi:10.1073/pnas.122206399.

Lev-Ram V, Mehta SB, Kleinfeld D, Tsien RY (2003) Reversing cerebellar long-term depression. Proc Natl Acad Sci U S A 100:15989-15993, doi:10.1073/pnas.2636935100.

Linden DJ (2003) Neuroscience. From molecules to memory in the cerebellum. Science 301:1682-1685, doi:10.1126/science.1090462.

Lisberger SG (1998) Physiologic basis for motor learning in the vestibulo-ocular reflex. Otolaryngol Head Neck Surg 119:43-48, doi:10.1016/S0194-5998(98)70172-X.

Lisberger SG, Fuchs AF (1978) Role of primate flocculus during rapid behavioral modification of vestibuloocular reflex. I. Purkinje cell activity during visually guided horizontal smooth-pursuit eye movements and passive head rotation. J Neurophysiol 41:733-763, doi:10.1152/jn.1978.41.3.733.

Lisberger SG, Miles FA (1980) Role of primate medial vestibular nucleus in long-term adaptive plasticity of vestibuloocular reflex. J Neurophysiol 43:1725-1745, doi:10.1152/jn.1980.43.6.1725.

Llinás RR (2011) Cerebellar motor learning versus cerebellar motor timing: the climbing fibre story. J Physiol 589:3423-3432, doi:10.1113/jphysiol.2011.207464.

Loewenstein Y, Mahon S, Chadderton P, Kitamura K, Sompolinsky H, Yarom Y, Häusser M (2005) Bistability of cerebellar Purkinje cells modulated by sensory stimulation. Nat Neurosci 8:202-211, doi:10.1038/nn1393.

Ly R, Bouvier G, Schonewille M, Arabo A, Rondi-Reig L, Léna C, Casado M, De Zeeuw CI, Feltz A (2013) T-type channel blockade impairs long-term potentiation at the parallel fiber-Purkinje cell synapse and cerebellar learning. Proc Natl Acad Sci U S A 110:20302-20307, doi:10.1073/pnas.1311686110.

Mathy A, Ho SSN, Davie JT, Duguid IC, Clark BA, Häusser M (2009) Encoding of oscillations by axonal bursts in inferior olive neurons. Neuron 62:388-399, doi:10.1016/j.neuron.2009.03.023.

McElvain LE, Friedman B, Karten HJ, Svoboda K, Wang F, Deschênes M, Kleinfeld D (2018) Circuits in the rodent brainstem that control whisking in concert with other orofacial motor actions. Neuroscience 368:152-170, doi:10.1016/j.neuroscience.2017.08.034.

Medina JF, Lisberger SG (2007) Variation, signal, and noise in cerebellar sensory-motor processing for smooth-pursuit eye movements. J Neurosci 27:6832-6842, doi:10.1523/JNEUROSCI.1323-07.2007.

Medina JF, Lisberger SG (2008) Links from complex spikes to local plasticity and motor learning in the cerebellum of awake-behaving monkeys. Nat Neurosci 11:1185-1192, doi:10.1038/nn.2197.

Moreno-Paublete R, Canlon B, Cederroth CR (2017) Differential neural responses underlying the inhibition of the startle response by pre-pulses or gaps in mice. Front Cell Neurosci 11:19, doi:10.3389/fncel.2017.00019.

Mukamel EA, Nimmerjahn A, Schnitzer MJ (2009) Automated analysis of cellular signals from large-scale calcium imaging data. Neuron 63:747-760, doi:10.1016/j.neuron.2009.08.009.

Ohtsuki G, Piochon C, Hansel C (2009) Climbing fiber signaling and cerebellar gain control. Front Cell Neurosci 3:4, doi:10.3389/neuro.03.004.2009.

Ozden I, Sullivan MR, Lee HM, Wang SSH (2009) Reliable coding emerges from coactivation of climbing fibers in microbands of cerebellar Purkinje neurons. J Neurosci 29:10463-10473, doi:10.1523/JNEUROSCI.0967-09.2009.

Ozden I, Dombeck DA, Hoogland TM, Tank DW, Wang SS (2012) Widespread state-dependent shifts in cerebellar activity in locomoting mice. PLoS One 7:e42650, doi:10.1371/journal.pone.0042650.

Perkon I, Kosir A, Itskov PM, Tasic J, Diamond ME (2011) Unsupervised quantification of whisking and head movement in freely moving rodents. J Neurophysiol 105:1950-1962, doi:10.1152/jn.00764.2010.

Peter S, Ten Brinke MM, Stedehouder J, Reinelt CM, Wu B, Zhou H, Zhou K, Boele HJ, Kushner SA, Lee MG, Schmeisser MJ, Boeckers TM, Schonewille M, Hoebeek FE, De Zeeuw CI (2016) Dysfunctional cerebellar Purkinje cells contribute to autism-like behaviour in *Shank2*-deficient mice. Nat Commun 7:12627, doi:10.1038/ncomms12627.

Petersen CCH (2014) Cortical control of whisker movement. Annu Rev Neurosci 37:183-203, doi:10.1146/annurev-neuro-062012-170344.

Petreanu L, Gutnisky DA, Huber D, Xu NL, O'Connor DH, Tian L, Looger L, Svoboda K (2012) Activity in motor-sensory projections reveals distributed coding in somatosensation. Nature 489:299-303, doi:10.1038/nature11321.

Popa LS, Hewitt AL, Ebner TJ (2012) Predictive and feedback performance errors are signaled in the simple spike discharge of individual Purkinje cells. J Neurosci 32:15345-15358, doi:10.1523/JNEUROSCI.2151-12.2012.

Prescott TJ, Diamond ME, Wing AM (2011) Active touch sensing. Philos Trans R Soc Lond B Biol Sci 366:2989-2995, doi:10.1098/rstb.2011.0167.

Proville RD, Spolidoro M, Guyon N, Dugué GP, Selimi F, Isope P, Popa D, Léna C (2014) Cerebellum involvement in cortical sensorimotor circuits for the control of voluntary movements. Nat Neurosci 17:1233-1239, doi:10.1038/nn.3773.

Rahmati N, Owens CB, Bosman LWJ, Spanke JK, Lindeman S, Gong W, Potters JW, Romano V, Voges K, Moscato L, Koekkoek SKE, Negrello M, De Zeeuw CI (2014) Cerebellar potentiation and

learning a whisker-based object localization task with a time response window. J Neurosci 34:1949-1962, doi:10.1523/JNEUROSCI.2966-13.2014.

Ramakrishnan KB, Voges K, De Propris L, De Zeeuw CI, D'Angelo E (2016) Tactile stimulation evokes long-lasting potentiation of Purkinje cell discharge *in vivo*. Front Cell Neurosci 10:36, doi:10.3389/fncel.2016.00036.

Ruigrok TJH, Teune TM, van der Burg J, Sabel-Goedknegt H (1995) A retrograde double-labeling technique for light microscopy. A combination of axonal transport of cholera toxin B-subunit and a gold-lectin conjugate. J Neurosci Methods 61:127-138, doi:10.1016/0165-0270(94)00034-E.

Sanchis-Segura C, Borchardt T, Vengeliene V, Zghoul T, Bachteler D, Gass P, Sprengel R, Spanagel R (2006) Involvement of the AMPA receptor GluR-C subunit in alcohol-seeking behavior and relapse. J Neurosci 26:1231-1238, doi:10.1523/JNEUROSCI.4237-05.2006.

Schonewille M, Gao Z, Boele HJ, Vinueza-Veloz MF, Amerika WE, Simek AAM, De Jeu MT, Steinberg JP, Takamiya K, Hoebeek FE, Linden DJ, Huganir RL, De Zeeuw CI (2011) Reevaluating the role of LTD in cerebellar motor learning. Neuron 70:43-50, doi:10.1016/j.neuron.2011.02.044.

Schonewille M, Belmeguenai A, Koekkoek SK, Houtman SH, Boele HJ, van Beugen BJ, Gao Z, Badura A, Ohtsuki G, Amerika WE, Hosy E, Hoebeek FE, Elgersma Y, Hansel C, De Zeeuw CI (2010) Purkinje cell-specific knockout of the protein phosphatase PP2B impairs potentiation and cerebellar motor learning. Neuron 67:618-628, doi:10.1016/j.neuron.2010.07.009.

Schultz SR, Kitamura K, Post-Uiterweer A, Krupic J, Häusser M (2009) Spatial pattern coding of sensory information by climbing fiber-evoked calcium signals in networks of neighboring cerebellar Purkinje cells. J Neurosci 29:8005-8015, doi:10.1523/jneurosci.4919-08.2009.

Shin SL, Hoebeek FE, Schonewille M, De Zeeuw CI, Aertsen A, De Schutter E (2007) Regular patterns in cerebellar Purkinje cell simple spike trains. PLoS One 2:e485, doi:10.1371/journal.pone.0000485.

Simony E, Bagdasarian K, Herfst L, Brecht M, Ahissar E, Golomb D (2010) Temporal and spatial characteristics of vibrissa responses to motor commands. J Neurosci 30:8935-8952, doi:10.1523/JNEUROSCI.0172-10.2010.

Simpson JI, Wylie DR, De Zeeuw CI (1996) On climbing fiber signals and their consequence(s). Behav Brain Sci 19:384-398, doi:10.1017/S0140525X00081486.

Staudacher EM, Gebhardt M, Dürr V (2005) Antennal movements and mechanoreception: Neurobiology of active tactile sensors. Adv Insect Physiol 32:49-205, doi:10.1016/S0065-2806(05)32002-9.

Stone LS, Lisberger SG (1990) Visual responses of Purkinje cells in the cerebellar flocculus during smooth-pursuit eye movements in monkeys. II. Complex spikes. J Neurophysiol 63:1262-1275, doi:10.1152/jn.1990.63.5.1262.

Streng ML, Popa LS, Ebner TJ (2018) Modulation of sensory prediction error in Purkinje cells during visual feedback manipulations. Nat Commun 9:1099, doi:10.1038/s41467-018-03541-0.

Sugihara I, Quy PN (2007) Identification of aldolase C compartments in the mouse cerebellar cortex by olivocerebellar labeling. J Comp Neurol 500:1076-1092, doi:10.1002/cne.21219.

Swerdlow NR, Caine SB, Braff DL, Geyer MA (1992) The neural substrates of sensorimotor gating of the startle reflex: a review of recent findings and their implications. J Psychopharmacol 6:176-190, doi:10.1177/026988119200600210.

Ten Brinke MM, Boele HJ, Spanke JK, Potters JW, Kornysheva K, Wulff P, IJpelaar ACHG, Koekkoek SKE, De Zeeuw CI (2015) Evolving models of Pavlovian conditioning: cerebellar cortical dynamics in awake behaving mice. Cell Rep 13:1977-1988, doi:10.1016/j.celrep.2015.10.057.

Teune TM, van der Burg J, van der Moer J, Voogd J, Ruigrok TJ (2000) Topography of cerebellar nuclear projections to the brain stem in the rat. Prog Brain Res 124:141-172, doi:10.1016/S0079-6123(00)24014-4.

Thier P, Dicke PW, Haas R, Thielert CD, Catz N (2002) The role of the oculomotor vermis in the control of saccadic eye movements. Ann N Y Acad Sci 978:50-62, doi:10.1111/j.1749-6632.2002.tb07555.x.

Tsutsumi S, Yamazaki M, Miyazaki T, Watanabe M, Sakimura K, Kano M, Kitamura K (2015) Structure-Function Relationships between Aldolase C/Zebrin II Expression and Complex Spike Synchrony in the Cerebellum. J Neurosci 35:843-852, doi:10.1523/JNEUROSCI.2170-14.2015.

Van Der Giessen RS, Koekkoek SK, van Dorp S, De Gruijl JR, Cupido A, Khosrovani S, Dortland B, Wellershaus K, Degen J, Deuchars J, Fuchs EC, Monyer H, Willecke K, De Jeu MTG, De Zeeuw CI (2008) Role of olivary electrical coupling in cerebellar motor learning. Neuron 58:599-612, doi:10.1016/j.neuron.2008.03.016.

Voges K, Wu B, Post L, Schonewille M, De Zeeuw CI (2017) Mechanisms underlying vestibulo-cerebellar motor learning in mice depend on movement direction. J Physiol 595:5301-5326, doi:10.1113/JP274346.

Voigts J, Herman DH, Celikel T (2015) Tactile object localization by anticipatory whisker motion. J Neurophysiol 113:620-632, doi:10.1152/jn.00241.2014.

Voogd J, Glickstein M (1998) The anatomy of the cerebellum. Trends Neurosci 21:370-375, doi:10.1016/S0166-2236(98)01318-6.

Waespe W, Cohen B, Raphan T (1985) Dynamic modification of the vestibulo-ocular reflex by the nodulus and uvula. Science 228:199-202, doi:10.1126/science.3871968

Welker WI (1964) Analysis of sniffing of the albino rat. Behaviour 22:223-244,

Welsh JP, Lang EJ, Suglhara I, Llinas R (1995) Dynamic organization of motor control within the olivocerebellar system. Nature 374:453-457, doi:10.1038/374453a0.

Witter L, Canto CB, Hoogland TM, de Gruijl JR, De Zeeuw CI (2013) Strength and timing of motor responses mediated by rebound firing in the cerebellar nuclei after Purkinje cell activation. Front Neural Circuits 7:133, doi:10.3389/fncir.2013.00133.

Wolpert DM, Miall RC, Kawato M (1998) Internal models in the cerebellum. Trends Cogn Sci 2:338-347, doi:10.1016/S1364-6613(98)01221-2.

Woolsey TA, Welker C, Schwartz RH (1975) Comparative anatomical studies of the SmI face cortex with special reference to the occurrence of "barrels" in layer IV. J Comp Neurol 164:79-94, doi:10.1002/cne.901640107.

Yamamoto T, Fukuda M, Llinás R (2001) Bilaterally synchronous complex spike Purkinje cell activity in the mammalian cerebellum. Eur J Neurosci 13:327-339, doi:10.1046/j.0953-816X.2000.01395.x.

Yang Y, Lisberger SG (2014) Purkinje-cell plasticity and cerebellar motor learning are graded by complex-spike duration. Nature 510:529-532, doi:10.1038/nature13282.

Yang Y, Lisberger SG (2017) Modulation of complex-spike duration and probability during cerebellar motor learning in visually guided smooth-pursuit eye movements of monkeys. eNeuro 4, doi:10.1523/ENEURO.0115-17.2017.

Zeng H, Chattarji S, Barbarosie M, Rondi-Reig L, Philpot BD, Miyakawa T, Bear MF, Tonegawa S (2001) Forebrain-specific calcineurin knockout selectively impairs bidirectional synaptic plasticity and working/episodic-like memory. Cell 107:617-629, doi:10.1016/S0092-8674(01)00585-2.

Zhou H, Lin Z, Voges K, Ju C, Gao Z, Bosman LWJ, Ruigrok TJH, Hoebeek FE, De Zeeuw CI, Schonewille M (2014) Cerebellar modules operate at different frequencies. eLIFE 3:e02536, doi:10.7554/eLife.02536.

Figure legends

Figure 1 | Whisker pad stimulation triggers stereotypic whisker behavior

A. Mouse head with unclipped large facial whiskers and the location of the air puffer. **B.** After pre-processing, whiskers were recognized by the tracking algorithm. Individual whiskers are color-coded. **C.** Air puff stimulation triggered stereotypic whisker movements consisting of an initial passive backwards movement followed by active protraction. Deflection angles of individually tracked whiskers are denoted in distinct colors (same color scheme as in panel **B**). **D.** The mean whisker angle during 0.5 Hz air puff stimulation of the whisker pad from a representative mouse. During approximately half the trials, the active protraction was only a single sweep; in the other traces multiple sweeps were observed. Prolonged periods of active whisking were rare. A trial with (**E**) and another one without (**F**) prolonged movements are enlarged. **G.** To indicate the variability in whisker behavior, 100 trials of the experiment illustrated above were superimposed. The thick line indicates the median. **H.** Violin plots showing the amplitudes (difference between maximal retraction and maximal protraction in the indicated 200 ms intervals (see panel **G**)) of individual trials of 16 mice (with approximately 100 trials per mouse). Horizontal lines represent 10th, 25th, 50th, 75th and 90th percentiles. Top: Fractions of trials with movements exceeding 10°. Asterisks indicate significantly different fractions of trials with movement. *** $p < 0.001$ ($\chi^2 = 1470.24$; 3x2 $\chi 2$ test).

Figure 2 | Air puffs induce reflexive whisker movements

A. Schematic drawing of the experimental layout. Air puffs lasting 30 ms were delivered from three different locations. In addition, some air puffs delivered ipsilaterally from the front were preceded by a brief air puff (2 ms) 100 ms before the actual air puff to test for pre-pulse

inhibition (PPI). The four stimulus conditions were applied in a random order. **B.** For each of the 9 mice tested, we calculated the average whisker response (on the ipsilateral side) and represented these as summed line plots. The stacked line plots are scaled such that the brightest line (on top) depicts the average of all mice. The insets show the duration of the retraction (until the whiskers reached the baseline position again) comparing the 2 ms and the 30 ms pulses (left) and the maximal protraction amplitudes upon the pre-pulse compared to the pulse (right). The passive retraction upon the short pre-pulse was less intense, but the consecutive protractions were of similar amplitude, indicating the absence of pre-pulse inhibition (p = 0.0078 and p = 0.4961, respectively; Wilcoxon matched-pairs tests; significance level = 0.025 after Bonferroni correction for multiple comparisons). **C.** Overlay of averaged ipsilateral whisker responses with shaded areas indicating ± SEM. The three ipsilateral conditions resulted in similar amounts of protraction. Note that the puff from the back did not cause a retraction preceding the protraction and that the pre-pulse did not affect the size of the protraction following the second air puff. The brief pre-pulse induced a shorter retraction, but this had no effect on the protraction. Air puffs to the contralateral whisker pad caused stronger protractions than the ipsilateral stimuli. **D.** The maximum retraction was largest when the air puffer was in front of the ipsilateral whiskers. The shorter pre-pulse did cause a briefer retraction (see inset in **B**), but the amplitude was not significantly different from the retraction caused by the longer pulse (p = 0.268; Dunn's pair-wise post-hoc test after Friedman's two-way ANOVA; see Table S1). Puffing from the contralateral whiskers or the ipsilateral whiskers from the back caused the least retraction, indicating that the initial retraction is largely passive and caused by the air flow of the stimulator. **E.** The maximum protraction reached was similar for all conditions, except in case the contralateral whiskers were stimulated, which led to a stronger protraction on the ipsilateral side. n.s. $p > 0.05$; * $p < 0.05$; *** $p < 0.001$; *** $p < 0.001$. See also Source Data file.

Figure 3 | Anatomical distribution of Purkinje cell responses to whisker pad stimulation

A. Representative extracellular recording of a Purkinje cell in an awake mouse. The vertical lines represent simple spikes. This traces contains a single complex spike that is indicated by a blue dot above the trace. **B.** Complex spike responses of the same Purkinje cell to air puff stimulation of the whisker pad. **C.** The latencies vs. the peak of the complex spike responses of all 118 Purkinje cells with a significant complex spike response. Note that a minority of the Purkinje cells showed relatively long latency times. **D.** Simple spike responses of the same Purkinje cell as in panels **A** and **B**. Note that the simple spike firing frequency is about 60-70 Hz. **E.** Peak amplitudes and peak latency times of simple spike responses (bottom) of all 127 Purkinje cells showing a significant simple spike response to whisker pad stimulation. Simple spike responses were often found to be bi-phasic. The closed circles reflect the first and the open symbols the second phase of the simple spike response. Non-significant responses are omitted. F. Simplified scheme of the somatosensory pathways from the whisker pad to the cerebellar Purkinje cells (PCs) and of the motor pathways directing whisker movement. The information flows from the whisker pad via the trigeminal nuclei and the thalamus to the primary somatosensory (S1) and motor cortex (M1). S1 and M1 project to the inferior olive via the nuclei of the meso-diencephalic junction (MDJ) and to the pontine nuclei. Both the inferior olive and the pontine nuclei also receive direct inputs from the trigeminal nuclei. The mossy fibers (MF) from the pontine nuclei converge with direct trigeminal MF on the cerebellar granule cells (GrC) that send parallel fibers (PF) to the PCs. The inferior olive provides climbing fibers (CF) that form extraordinarily strong synaptic connections with the PCs. Both the PFs and the CFs also drive feedforward inhibition to PCs via molecular layer interneurons (MLI). The GABAergic PCs provide the sole output of the cerebellar cortex that is directed to the cerebellar nuclei (CN). The CN sends the cerebellar output both upstream via the thalamus back to the cerebral cortex and downstream to motor areas in the brainstem

and spinal cord. The whisker pad muscles are under control of the facial nucleus which is mainly innervated via the reticular formation. Several feedback loops complement these connections. For references, see Bosman et al. (2011) and Deschênes et al. (2016). **G.** For most of the PC recordings in this study, the anatomical locations were defined by a combination of surface photographs and electrolytic lesions made after completion of the recordings. An example of such a lesion in crus 1 is shown here in combination with a Nissl staining. SL = simple lobule. **H**. Heat map showing the anatomical distribution of the strength of the complex spike responses projected on the surface of crus 1 and crus 2. The locations of all 132 recorded Purkinje cells were attributed to a rectangular grid. The average complex spike response strength was calculated per grid position and averaged between each grid position and its neighbor. The grey lines indicate the borders to the cerebellar zones (see Figure supplement 1I). **I.** The same for the variation in the first phase of the simple spike responses. Note that for the simple spikes the blue colors indicate suppression of firing rather than the absence of a response.

Figure 4 | Coherent complex spike firing is specifically enhanced by whisker pad stimulation

A. Field of view of a piece of crus 1 recorded using two-photon Ca^{2+} imaging in an awake mouse. The colored areas indicate 22 regions of interest, corresponding to Purkinje cell dendrites. The accompanying fluorescent traces show Ca^{2+} transients, which are most likely complex spikes (**B**; cf. Schultz et al., 2009). In the absence of tactile stimulation coherent activity of groups of Purkinje cells is rare. **C.** Following air puff stimulation of the whisker pad (brown vertical lines), complex spike coherence occurs often as illustrated by five responsive Purkinje cells recorded simultaneously. **D.** Composite peri-stimulus time histogram of all Purkinje cells in the field of view shown in panel **A**. The colors represent the

coherence of Purkinje cell firing, defined as the fraction of Purkinje cells active during each frame of 40 ms. Complex spike coherence is relatively rare during inter-trial intervals, but strongly enhanced following air puff stimulation. **E.** The same peri-stimulus histogram as in D, but with colors indicating the chance of occurrence of the level of coherence found based upon Poisson distribution of all complex spikes in this recording, emphasizing that coherence occurred more than expected, mainly during the sensory response. Indeed, during 1 Hz air puff stimulation, complex spikes were observed to be produced by large ensembles. In the absence of tactile stimulation, ensemble sizes tended to be smaller (**F**). The data presented in panels **D**-**F** come from the field of view shown in panel **A**. **G.** There was a shift from complex spikes fired by a single or a few Purkinje cells towards complex spikes fired by larger ensembles when introducing air puff stimulation. Presented are the median and the inter-quartile range of the differences between the two histograms as illustrated for an example experiment in panel **F** (n = 10). The increase in coherence directly after stimulation was highly significant (p = 0.001; Fr = 28.878; df = 9; Friedman's two-way ANOVA). * $p < 0.05$; ** $p < 0.01$, *** $p < 0.001$, **** $p < 0.0001$, ***** $p < 0.00001$.

Figure 5 | Larger whisker protractions are preferably preceded by a complex spike

A. Whisker traces according to the presence (violet) or the absence (magenta) of a complex spike (CS) produced by a simultaneously recorded Purkinje cell in the first 100 ms after stimulus onset. The trials with a complex spike tended to have a stronger protraction, which was also observed in the population of Purkinje cells with a significant complex spike response to air puff stimulation (n = 55) (**B**). **C.** Averaged convolved peri-stimulus time histograms of complex spikes (*blue*) and the averaged difference in whisker position (*purple*) between trials with and without complex spikes. Complex spikes precede the observed differences in movement. Shaded areas indicate s.d. (**A**) or SEM (**B** and **C**). **D.** Time intervals

between the peak of the complex spike response and the moment of maximal difference in whisker position between trials with and without complex spikes. **E.** Changes in average whisker angle before stimulation (period a; see time bar in panel **B**), in maximal retraction (period b) and in maximal protraction (period c) between trials with and without a complex spike in the 100 ms after an air puff. * $p > 0.05$; ** $p < 0.01$; *** $p < 0.001$.

Figure 6 | Increased simple spike firing correlates with whisker protraction

A. Changes in the instantaneous simple spike (SS) firing rate (convolved with a 6 ms Gaussian kernel; *blue*) correlate roughly with whisker movement (*purple*). This is illustrated with a representative recording of a Purkinje cell. Vertical brown lines indicate the moments of air puff stimulation to the (ipsilateral) whisker pad. The horizontal black line designates the interval expanded in **B**. Blue dots mark complex spikes. **C.** Correlation matrix showing a clear positive correlation of simple spike firing (blue trace at the bottom shows convolved peri-stimulus time histogram triggered on air puff stimulation) and whisker protraction (red trace at the left; indicated is the mean ± SEM of the whisker position) based on a trial-by-trial analysis. The correlation coefficient (R) over the dashed 45° line is shown at the bottom, together with the 99% confidence interval (*grey area*). These data correspond to the example Purkinje cell shown in **A**-**B**. Averaged data from all 25 Purkinje cells that displayed a significant correlation between simple spike rate and whisker position is shown in **D**. **E.** Scatter plots with linear regression lines show a positive correlation between whisker protraction and instantaneous SS firing as illustrated here for the Purkinje cell represented in panel C (R = 0.517; $p < 0.001$). Data are taken from the moment with the strongest correlation (150-160 ms after the onset of the air puff for both parameters). **F.** For all Purkinje cells with a significant correlation between whisker angle and simple spike rate, this correlation turned out to be positive when evaluating 100 trials for each of the 25 Purkinje cells (R = 0.199; $p <$

0.001; Pearson's correlation test). Shown is the linear regression line (*black*) and the 95% confidence intervals (*blue*). The experiments are normalized based upon their Z-score. Data are taken from the moment with the strongest correlation (120-130 ms (whiskers) vs. 140-150 ms (simple spikes)). Thus, increased simple spike firing correlates with whisker protraction. ** $p < 0.01$; *** $p < 0.001$.

Figure 7 | Contralateral whisker pad stimulation induces stronger whisker protraction and stronger simple spike responses

A. Whisker traces of a representative mouse following air puff stimulation of the ipsilateral (left panel) and contralateral (right panel) whisker pad (see scheme in **B**). Despite a similar strength of stimulation, the protraction of the whiskers was larger upon contralateral stimulation (cf. Figure 2). **C.** Stacked line plots of the averaged whisker traces of 9 mice with the difference between the contralateral and ipsilateral stimulation depicted in the third column. **D.** Complex spike responses, on the other hand, were more prominent upon ipsilateral stimulation. **E.** The observation that increased simple spike firing correlates to enhanced whisker protraction (cf. Figure 6) was confirmed under these experimental conditions. * $p < 0.05$; *** $p < 0.001$. See also Data Source File.

Figure 8 | 4 Hz tetanic stimulation leads to anticipation of the simple spike response and to stronger protraction of the whiskers

A. Induction protocol. Air puff stimulation at 0.5 Hz is used to characterize the impact of a brief period (20 s) of 4 Hz air puff stimulation. **B.** Stacked line plots (see Methods) showing the averaged whisker response before (1st column) and after (2nd column) 4 Hz sensory stimulation (n = 16 mice). The plots are sorted by increased protraction induced by 4 Hz tetanic stimulation (3rd column). Each color depicts one mouse. Plots are normalized so that

the most intense color represents the average. 4 Hz tetanic stimulation leads to a more protracted form of whisker movement (4th column). Similar plots for complex spikes (**C**, showing little change) and simple spikes (**D**, showing a clear increase in firing, especially during the early phase of the response). For comparison, the averages are superimposed in E (for y-scaling and variations refer to **B**-**D**). Trial-by-trial analysis of 14 Purkinje cells before and after 4 Hz tetanic stimulation (cf. Figure 6C-D) highlighting the anticipation of simple spike firing (**F**). The x-axis is based upon the instantaneous simple spike firing frequency and the y-axis upon whisker angle. After induction, the maximal correlation (R) between simple spikes and whisker angle (along dashed 45° line) shifts to an earlier time point after the air puff (3rd column; shaded areas indicate SEM). In addition, a clear correlation is found with simple spike firing leading whisker movement (yellow/red area expands above the 45° line in 2nd column as compared to the left column). Scale bar of the correlation matrices (left and middle) is at the right of the 3rd column. ** $p < 0.01$; *** $p < 0.001$. See also Table S2 and Source Data File.

Figure 9 | 4 Hz tetanic stimulation specifically potentiates simple spike firing in Purkinje cells with weak complex spike responses

A. Repeated sensory stimulation (Figure 8A) induced an increase in simple spike response to whisker pad stimulation, but not in all Purkinje cells (PCs). There was a clear negative correlation between the strength of the complex spike (CS) response and the potentiation of the simple spike response. Overall, there was potentiation in the Purkinje cells with weak complex spike responses, but not in the strong CS responders (cf. Figure 3 - Figure supplement 1E). **B.** Heat map showing the anatomical distribution of the strength of the simple spike increase projected on the surface of crus 1 and crus 2. The 55 Purkinje cells were attributed to a rectangular grid. The average simple spike response strength was calculated per

grid position and averaged between each grid position and its neighbor. The grey lines indicate the borders to the cerebellar zones (see Figure 3 - Figure supplement 2D). **C.** Heat map of the distribution of Purkinje cells based upon the correlation of their simple spike rate and whisker position (cf. Figure 6D). Note that the strongest increase of simple spike responses after 4 Hz tetanic stimulation occurs in the region that also displayed the strongest correlation between instantaneous simple spike rate and whisker position. **D.** Example PSTHs of the simple spike response to whisker pad air puff stimulation of representative Purkinje cells and how they changed over time, depicted as heat maps of the instantaneous simple spike frequency (**E**; see scale bar in **D**). The left column displays the data from a representative Purkinje cell with a weak complex spike response, the right column of one with a strong complex spike response. The induction period is indicated with "4 Hz". **F.** The number of simple spikes following an air puff stimulation increased in weakly responding Purkinje cells and this increase remained elevated until the end of the recording (at least 30 min). In contrast, this increase was not found in Purkinje cells with strong complex spike responses. * $p < 0.05$; ** $p < 0.01$; *** $p < 0.001$.

Figure 10 | Expression of PP2B in Purkinje cells is required for increased protraction and simple spike firing following 4 Hz tetanic stimulation

A. Schematic representation of the principal pathways regulating bidirectional plasticity at the parallel fiber (PF) to Purkinje cell (PC) synapses. The direction of PF-PC plasticity depends on the intracellular Ca^{2+} concentration ($[Ca^{2+}]_i$) that is largely determined by climbing fiber (CF) activity. Following CF activity, $[Ca^{2+}]_i$ raises rapidly and activates a phosphorylation cascade involving α-Ca^{2+}/calmodulin-dependent protein kinase II (CaMKIIA) and several other proteins eventually leading to internalization of AMPA receptors and consequently to long-term depression (LTD). PF volleys in the absence of CF activity, on the other hand,

result in a moderate increase in $[Ca^{2+}]_i$, activating a protein cascade involving protein phosphatase 2B (PP2B) that promotes the insertion of new AMPA receptors into the postsynaptic density, thereby leading to long-term potentiation (LTP) of the PF-PC synapse. GluA3 subunits are part of the postsynaptic AMPA receptors. **B.** Example of a representative mouse with the averaged whisker movements before and after theta sensory stimulation, showing a stronger protraction afterwards, as evidenced by the differences between post- and pre-induction compared to a bootstrap analysis on the normal variation in whisker movements (**C**; shade: 99% confidence interval). Although also differences were observed in L7-PP2B mutants, these did generally not exceed the expected variations (*right*). **D.** In 14 out of 16 wild-type mice more protraction than expected was observed, against in only 3 out of 13 L7-PP2B mutant mice (*pie charts*). Stacked line plots of whisker movement differences between post- and pre-induction for all mice. The plots are normalized so that the brightest line indicates the average per genotype. **E.** In contrast to simple spike responses in WT mice, those in L7-PP2B KO mice could not be potentiated by our 4 Hz tetanic stimulation protocol. This effect was stable, also during longer recordings. For this analysis, we selected those with weak complex spike responses, as the PCs with a weak complex spike response did not show increased simple spike firing after 4 Hz tetanic stimulation (see Figure 9A). * $p < 0.05$; ** $p < 0.01$; *** $p < 0.001$

Figure 11 | Expression of AMPA receptor GluA3 subunits in Purkinje cells is required for increased protraction and simple spike firing following 4 Hz tetanic stimulation

A. Example of a representative L7-GluA3 mutant mouse with the averaged whisker movements before and after 4 Hz tetanic stimulation, showing similar degrees of protraction. **B.** Overall, 4 Hz tetanic stimulation did not result in stronger whisker protraction in L7-GluA3 mutant mice as observed in WT mice (see Figure 8). This is illustrated with a stacked

line plot. **C.** Comparison of the average change in whisker angle over the 120 ms following the onset of the air puff shows enhanced protraction in WT (n = 16), but not in LTP-deficient mice - neither in L7-PP2B (n = 13) nor in L7-GluA3 (n = 6) mutants, pointing towards a central role for parallel fiber-to-Purkinje cell LTP for the enhanced protraction in WT mice following a brief period of 4 Hz tetanic stimulation. The horizontal lines indicate the medians and the 1st and 3rd quartiles. The lack of change in whisker protraction following 4 Hz tetanic stimulation was reflected in the lack of change in simple spike responses as illustrated in three representative Purkinje cells (cf. Figure 9D-E). On top are the peri-stimulus time histograms (**D**) followed by heat maps illustrating the instantaneous firing rate over time (**E**). The induction period is indicated with "4 Hz". F. Overall, WT Purkinje cells (n = 35) showed increased simple spike firing after 4 Hz stimulation, while those in L7-PP2B (n = 21) or L7-GluA3 (n = 13) mutant mice did not. For this analysis, we restricted ourselves to the Purkinje cells with weak complex spike responses as the Purkinje cells with strong complex spike responses did not show potentiation in the WT mice (see Figure 9A) and to the first 100 trials after induction. As shown in Figure 11E, the increase in simple spiking firing developed over time (in WT, but not in L7-PP2B mice). Directly following the induction period, the increase in simple spike firing was not yet maximal. * $p < 0.05$; ** $p < 0.01$. See also Source Data File.

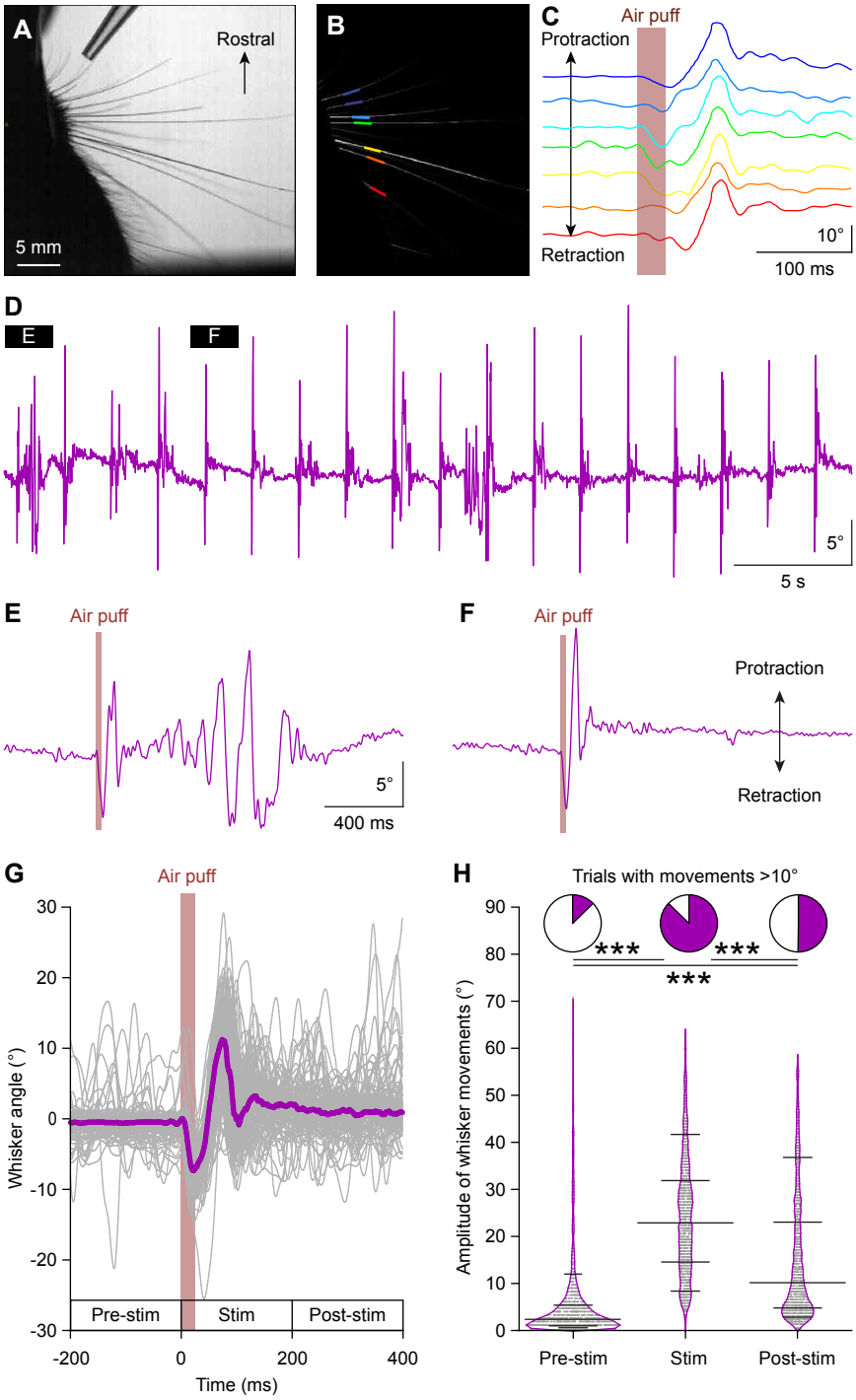

Figure 1 | Whisker pad stimulation triggers stereotypic whisker behavior
A. Mouse head with unclipped large facial whiskers and the location of the air puffer. **B.** After pre-processing, whiskers were recognized by the tracking algorithm. Individual whiskers are color-coded. **C.** Air puff stimulation triggered stereotypic whisker movements consisting of an initial passive backwards movement followed by active protraction. Deflection angles of individually tracked whiskers are denoted in distinct colors (same color scheme as in panel **B**). **D.** The mean whisker angle during 0.5 Hz air puff stimulation of the whisker pad from a representative mouse. During approximately half the trials, the active protraction was only a single sweep; in the other traces multiple sweeps were observed. Prolonged periods of active whisking were rare. A trial with (**E**) and another one without (**F**) prolonged movements are enlarged. **G.** To indicate the variability in whisker behavior, 100 trials of the experiment illustrated above were superimposed. The thick line indicates the median. **H.** Violin plots showing the amplitudes (difference between maximal retraction and maximal protraction in the indicated 200 ms intervals (see panel **G**)) of individual trials of 16 mice (with approximately 100 trials per mouse). Horizontal lines represent 10th, 25th, 50th, 75th and 90th percentiles. Top: Fractions of trials with movements exceeding 10°. Asterisks indicate significantly different fractions of trials with movement. *** $p < 0.001$ ($\chi^2 = 1470.24$; 3x2 χ^2 test).

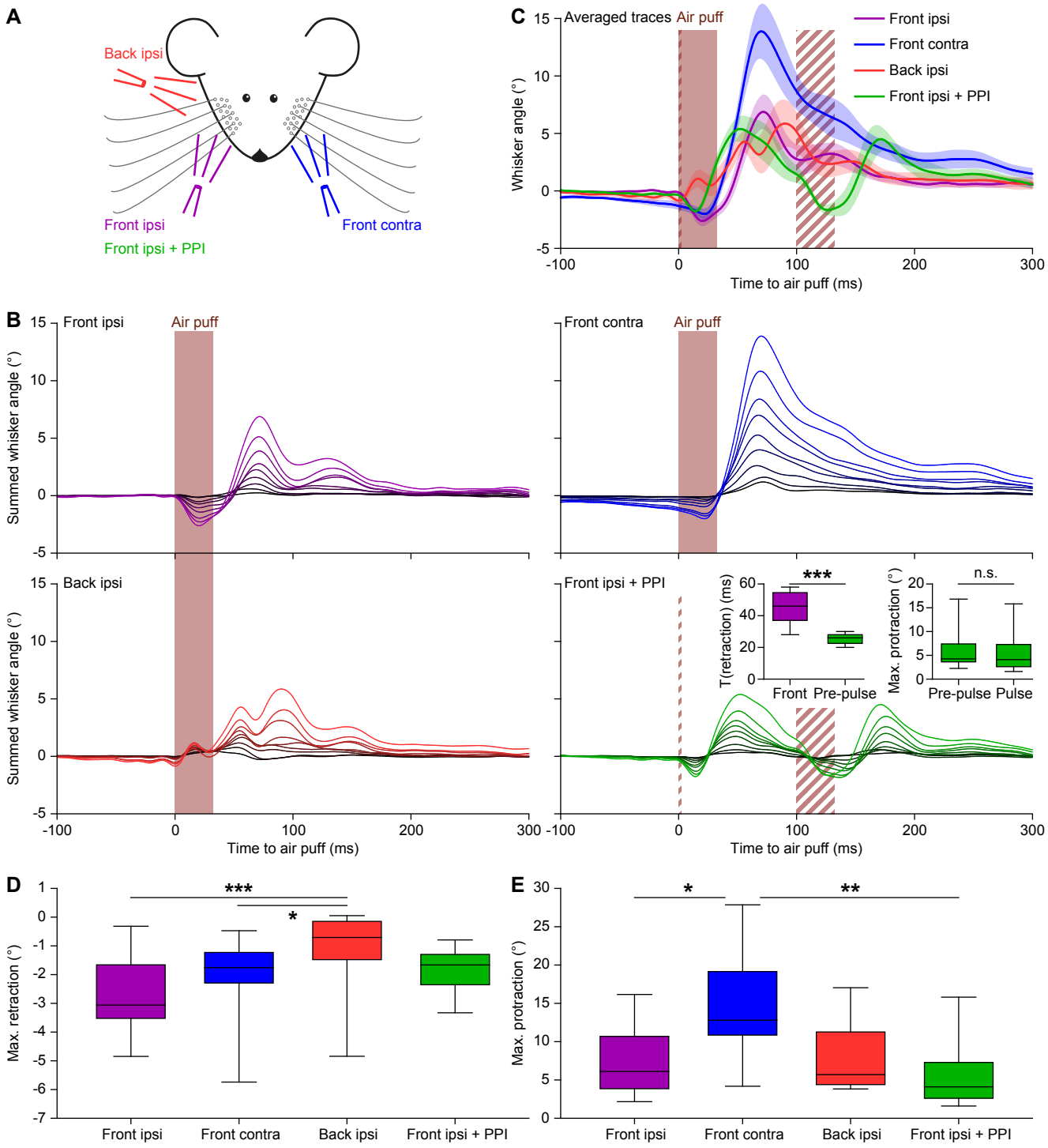

Figure 2 | Air puffs induce reflexive whisker movements
A. Schematic drawing of the experimental layout. Air puffs lasting 30 ms were delivered from three different locations. In addition, some air puffs delivered ipsilaterally from the front were preceded by a brief air puff (2 ms) 100 ms before the actual air puff to test for pre-pulse inhibition (PPI). The four stimulus conditions were applied in a random order. **B.** For each of the 9 mice tested, we calculated the average whisker response (on the ipsilateral side) and represented these as summed line plots. The stacked line plots are scaled such that the brightest line (on top) depicts the average of all mice. The *insets* show the duration of the retraction (until the whiskers reached the baseline position again) comparing the 2 ms and the 30 ms pulses (*left*) and the maximal protraction amplitudes upon the pre-pulse compared to the pulse (*right*). The passive retraction upon the short pre-pulse was less intense, but the consecutive protractions were of similar amplitude, indicating the absence of pre-pulse inhibition (p = 0.0078 and p = 0.4961, respectively; Wilcoxon matched-pairs tests; significance level = 0.025 after Bonferroni correction for multiple comparisons). **C.** Overlay of averaged ipsilateral whisker responses with shaded areas indicating ± SEM. The three ipsilateral conditions resulted in similar amounts of protraction. Note that the puff from the back did not cause a retraction preceding the protraction and that the pre-pulse did not affect the size of the protraction following the second air puff. The brief pre-pulse induced a shorter retraction, but this had no effect on the protraction. Air puffs to the contralateral whisker pad caused stronger protractions than the ipsilateral stimuli. **D.** The maximum retraction was largest when the air puffer was in front of the ipsilateral whiskers. The shorter pre-pulse did cause a briefer retraction (see inset in **B**), but the amplitude was not significantly different from the retraction caused by the longer pulse (p = 0.268; Dunn's pair-wise post-hoc test after Friedman's two-way ANOVA; see Table S1). Puffing from the contralateral whiskers or the ipsilateral whiskers from the back caused the least retraction, indicating that the initial retraction is largely passive and caused by the air flow of the stimulator. **E.** The maximum protraction reached was similar for all conditions, except in case the contralateral whiskers were stimulated, which led to a stronger protraction on the ipsilateral side. n.s. $p > 0.05$; * $p < 0.05$; *** $p < 0.001$; *** $p < 0.001$. See also Source Data file.

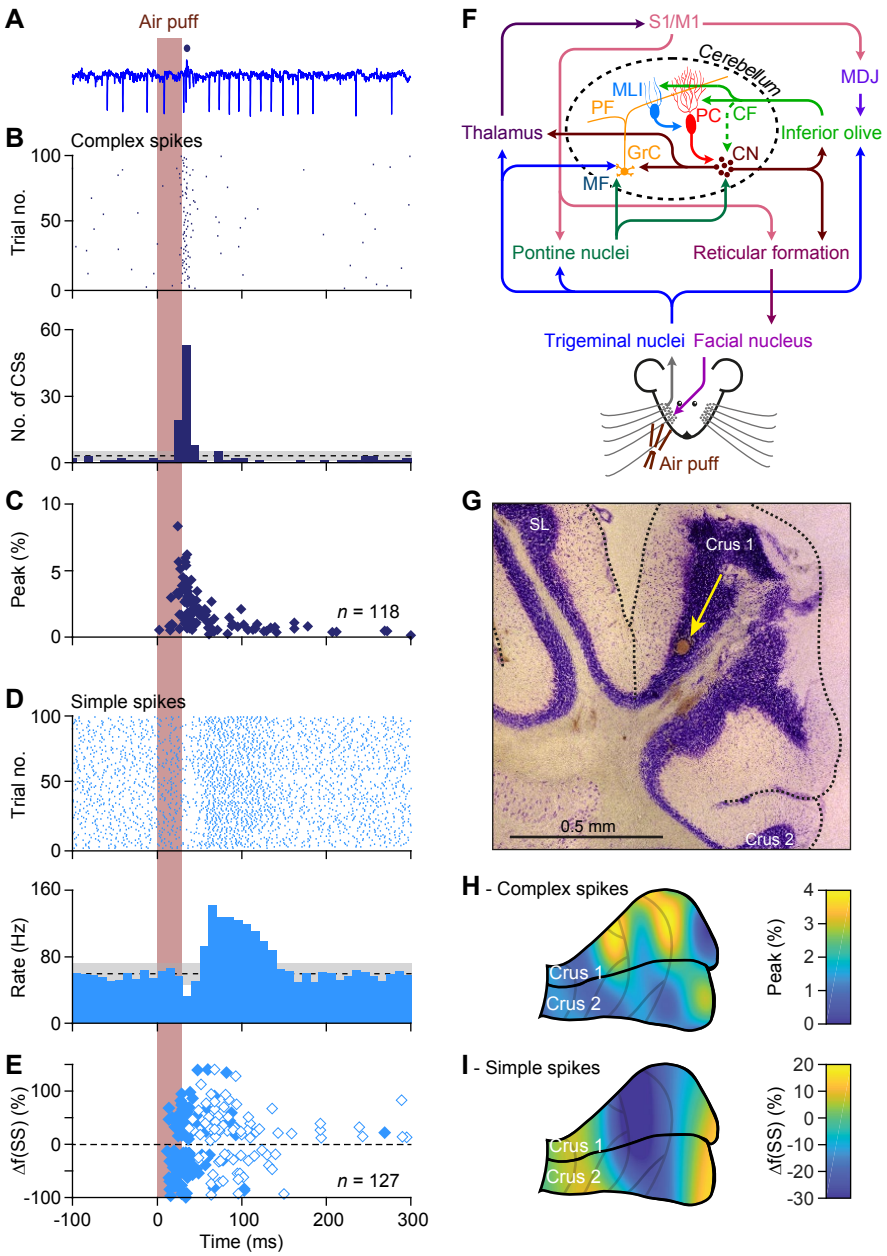

Figure 3 | Anatomical distribution of Purkinje cell responses to whisker pad stimulation

A. Representative extracellular recording of a Purkinje cell in an awake mouse. The vertical lines represent simple spikes. This traces contains a single complex spike that is indicated by a blue dot above the trace. **B.** Complex spike responses of the same Purkinje cell to air puff stimulation of the whisker pad. **C.** The latencies vs. the peak of the complex spike responses of all 118 Purkinje cells with a significant complex spike response. Note that a minority of the Purkinje cells showed relatively long latency times. **D.** Simple spike responses of the same Purkinje cell as in panels **A** and **B**. Note that the simple spike firing frequency is about 60-70 Hz. **E.** Peak amplitudes and peak latency times of simple spike responses (bottom) of all 127 Purkinje cells showing a significant simple spike response to whisker pad stimulation. Simple spike responses were often found to be bi-phasic. The closed circles reflect the first and the open symbols the second phase of the simple spike response. Non-significant responses are omitted. **F.** Simplified scheme of the somatosensory pathways from the whisker pad to the cerebellar Purkinje cells (PCs) and of the motor pathways directing whisker movement. The information flows from the whisker pad via the trigeminal nuclei and the thalamus to the primary somatosensory (S1) and motor cortex (M1). S1 and M1 project to the inferior olive via the nuclei of the meso-diencephalic junction (MDJ) and to the pontine nuclei. Both the inferior olive and the pontine nuclei also receive direct inputs from the trigeminal nuclei. The mossy fibers (MF) from the pontine nuclei converge with direct trigeminal MF on the cerebellar granule cells (GrC) that send parallel fibers (PF) to the PCs. The inferior olive provides climbing fibers (CF) that form extraordinarily strong synaptic connections with the PCs. Both the PFs and the CFs also drive feedforward inhibition to PCs via molecular layer interneurons (MLI). The GABAergic PCs provide the sole output of the cerebellar cortex that is directed to the cerebellar nuclei (CN). The CN sends the cerebellar output both upstream via the thalamus back to the cerebral cortex and downstream to motor areas in the brainstem and spinal cord. The whisker pad muscles are under control of the facial nucleus which is mainly innervated via the reticular formation. Several feedback loops complement these connections. For references, see Bosman et al. (2011) and Deschênes et al. (2016). **G.** For most of the PC recordings in this study, the anatomical locations were defined by a combination of surface photographs and electrolytic lesions made after completion of the recordings. An example of such a lesion in crus 1 is shown here in combination with a Nissl staining. SL = simple lobule. **H.** Heat map showing the anatomical distribution of the strength of the complex spike responses projected on the surface of crus 1 and crus 2. The locations of all 132 recorded Purkinje cells were attributed to a rectangular grid. The average complex spike response strength was calculated per grid position and averaged between each grid position and its neighbor. The grey lines indicate the borders to the cerebellar zones (see Figure supplement 1I). **I.** The same for the variation in the first phase of the simple spike responses. Note that for the simple spikes the blue colors indicate suppression of firing rather than the absence of a response.

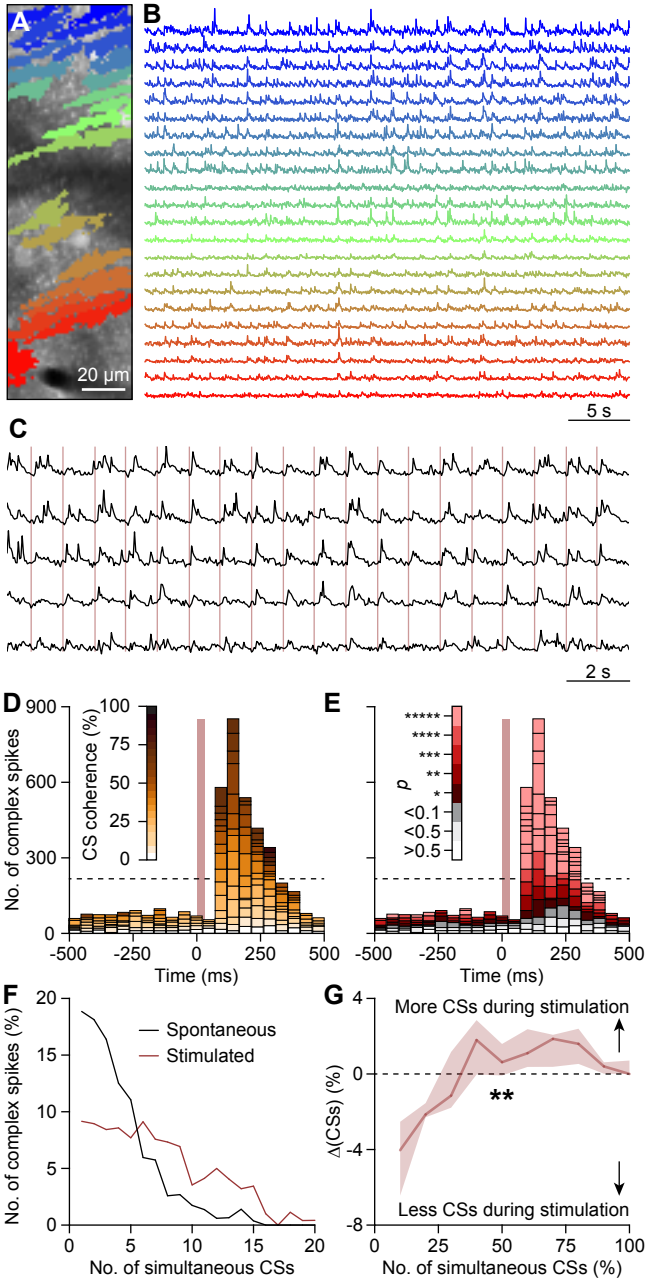

Figure 4 | Coherent complex spike firing is specifically enhanced by whisker pad stimulation

A. Field of view of a piece of crus 1 recorded using two-photon Ca^{2+} imaging in an awake mouse. The colored areas indicate 22 regions of interest, corresponding to Purkinje cell dendrites. The accompanying fluorescent traces show Ca^{2+} transients, which are most likely complex spikes (**B**; cf. Schultz et al., 2009). In the absence of tactile stimulation coherent activity of groups of Purkinje cells is rare. **C.** Following air puff stimulation of the whisker pad (brown vertical lines), complex spike coherence occurs often as illustrated by five responsive Purkinje cells recorded simultaneously. **D.** Composite peri-stimulus time histogram of all Purkinje cells in the field of view shown in panel **A**. The colors represent the coherence of Purkinje cell firing, defined as the fraction of Purkinje cells active during each frame of 40 ms. Complex spike coherence is relatively rare during inter-trial intervals, but strongly enhanced following air puff stimulation. **E**. The same peri-stimulus histogram as in **D**, but with colors indicating the chance of occurrence of the level of coherence found based upon Poisson distribution of all complex spikes in this recording, emphasizing that coherence occurred more than expected, mainly during the sensory response. Indeed, during 1 Hz air puff stimulation, complex spikes were observed to be produced by large ensembles. In the absence of tactile stimulation, ensemble sizes tended to be smaller (**F**). The data presented in panels **D**-**F** come from the field of view shown in panel **A**. **G**. There was a shift from complex spikes fired by a single or a few Purkinje cells towards complex spikes fired by larger ensembles when introducing air puff stimulation. Presented are the median and the inter-quartile range of the differences between the two histograms as illustrated for an example experiment in panel **F** (n = 10). The increase in coherence directly after stimulation was highly significant (p = 0.001; Fr = 28.878; df = 9; Friedman's two-way ANOVA).
* $p < 0.05$; ** $p < 0.01$, *** $p < 0.001$, **** $p < 0.0001$, ***** $p < 0.00001$.

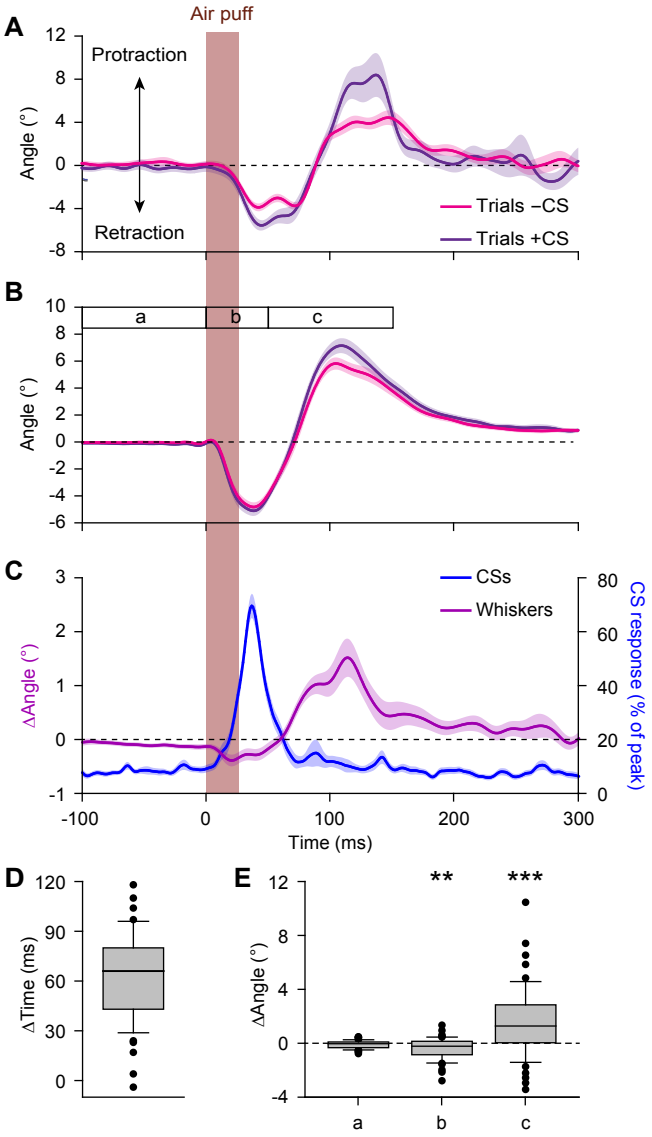

Figure 5 | Larger whisker protractions are preferably preceded by a complex spike

A. Whisker traces according to the presence (violet) or the absence (magenta) of a complex spike (CS) produced by a simultaneously recorded Purkinje cell in the first 100 ms after stimulus onset. The trials with a complex spike tended to have a stronger protraction, which was also observed in the population of Purkinje cells with a significant complex spike response to air puff stimulation (n = 55) (**B**). **C.** Averaged convolved peri-stimulus time histograms of complex spikes (blue) and the averaged difference in whisker position (purple) between trials with and without complex spikes. Complex spikes precede the observed differences in movement. Shaded areas indicate s.d. (**A**) or SEM (**B** and **C**). **D.** Time intervals between the peak of the complex spike response and the moment of maximal difference in whisker position between trials with and without complex spikes. **E.** Changes in average whisker angle before stimulation (period a; see time bar in panel **B**), in maximal retraction (period b) and in maximal protraction (period c) between trials with and without a complex spike in the 100 ms after an air puff. * $p > 0.05$; ** $p < 0.01$; *** $p < 0.001$.

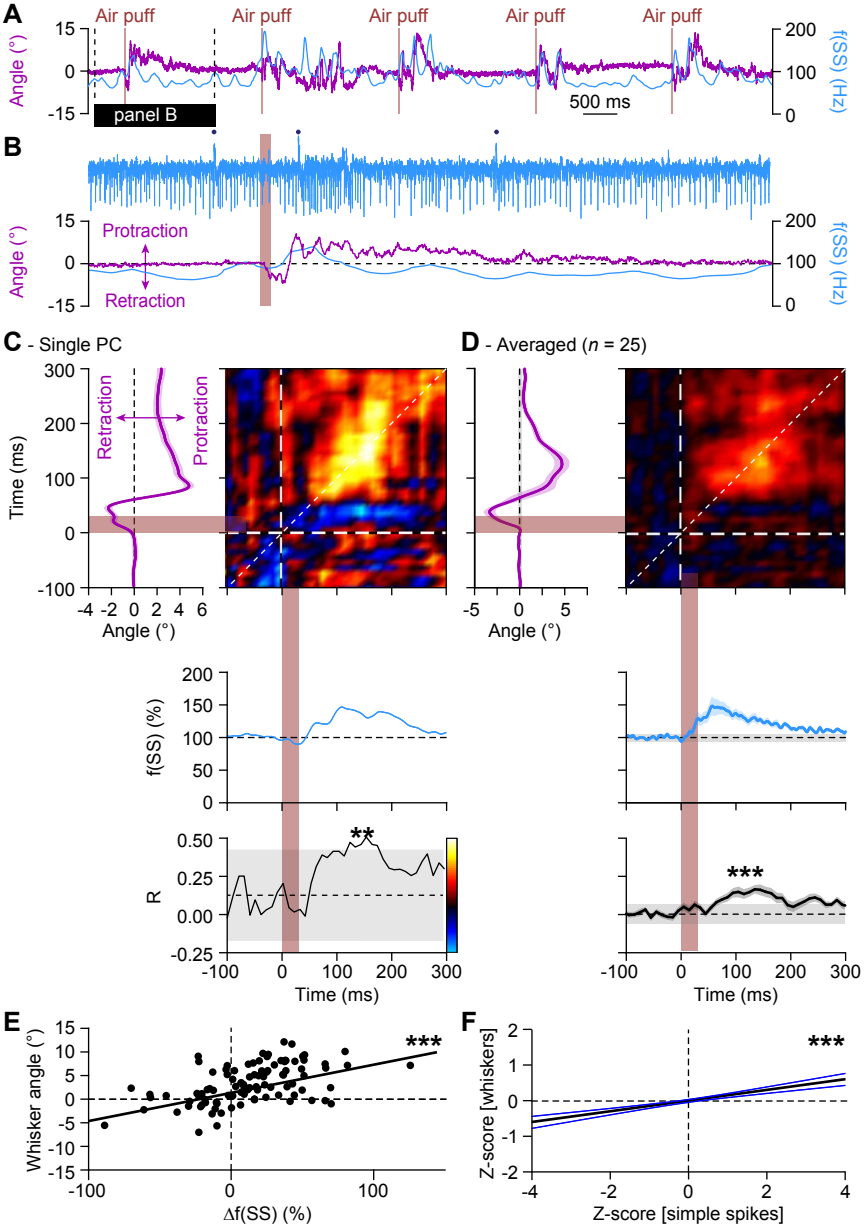

Figure 6 | Increased simple spike firing correlates with whisker protraction **A.** Changes in the instantaneous simple spike (SS) firing rate (convolved with a 6 ms Gaussian kernel; blue) correlate roughly with whisker movement (purple). This is illustrated with a representative recording of a Purkinje cell. Vertical brown lines indicate the moments of air puff stimulation to the (ipsilateral) whisker pad. The horizontal black line designates the interval expanded in **B**. Blue dots mark complex spikes. **C.** Correlation matrix showing a clear positive correlation of simple spike firing (blue trace at the bottom shows convolved peri-stimulus time histogram triggered on air puff stimulation) and whisker protraction (red trace at the left; indicated is the mean ± SEM of the whisker position) based on a trial-by-trial analysis. The correlation coefficient (R) over the dashed 45° line is shown at the bottom, together with the 99% confidence interval (grey area). These data correspond to the example Purkinje cell shown in **A**-**B**. Averaged data from all 25 Purkinje cells that displayed a significant correlation between simple spike rate and whisker position is shown in **D**. **E.** Scatter plots with linear regression lines show a positive correlation between whisker protraction and instantaneous SS firing as illustrated here for the Purkinje cell represented in panel **C** (R = 0.517; $p < 0.001$). Data are taken from the moment with the strongest correlation (150-160 ms after the onset of the air puff for both parameters). **F.** For all Purkinje cells with a significant correlation between whisker angle and simple spike rate, this correlation turned out to be positive when evaluating 100 trials for each of the 25 Purkinje cells (R = 0.199; $p < 0.001$; Pearson's correlation test). Shown is the linear regression line (*black*) and the 95% confidence intervals (*blue*). The experiments are normalized based upon their Z-score. Data are taken from the moment with the strongest correlation (120-130 ms (whiskers) vs. 140-150 ms (simple spikes)). Thus, increased simple spike firing correlates with whisker protraction.** $p < 0.01$; *** $p < 0.001$.

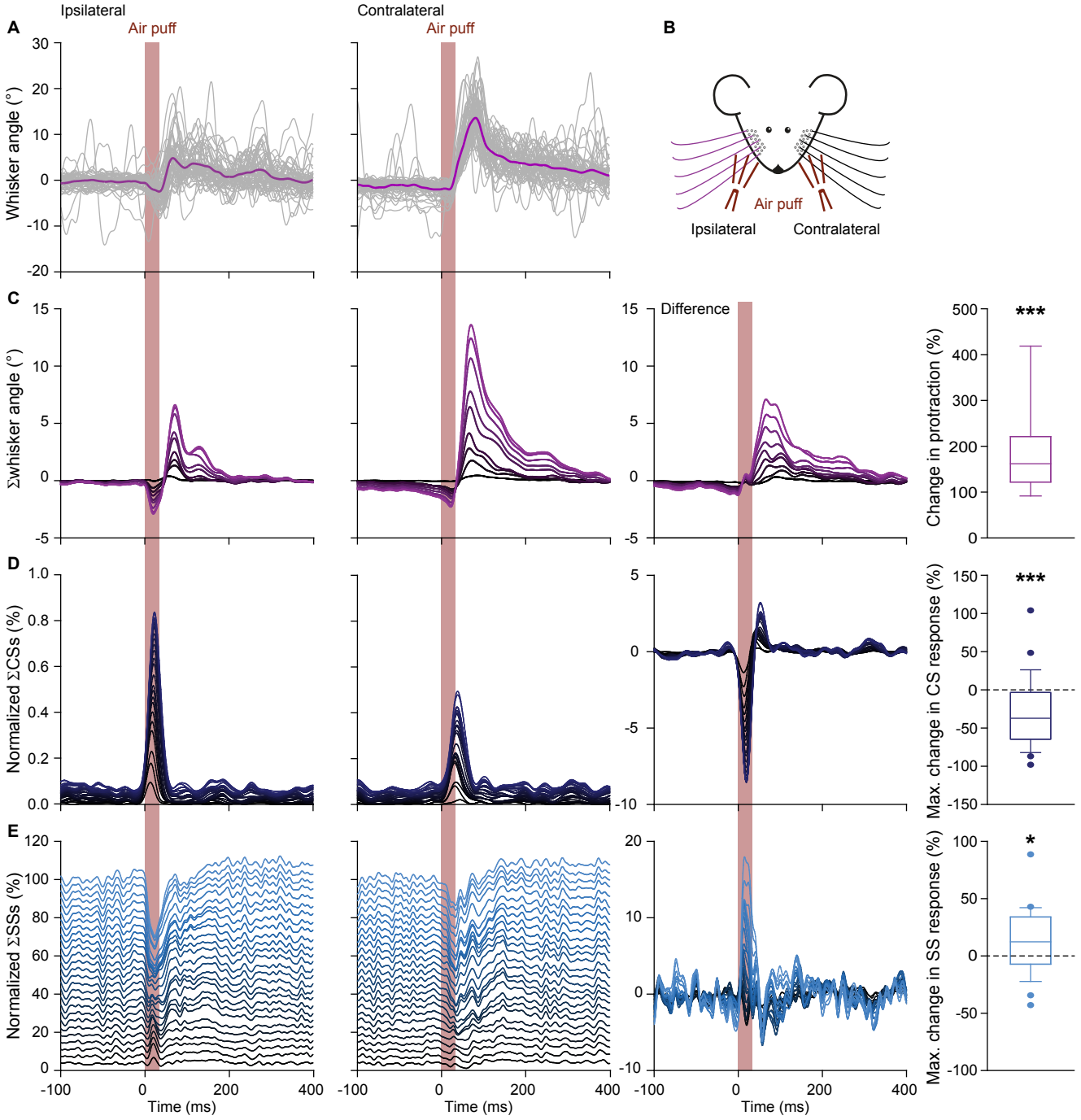

Figure 7 | Contralateral whisker pad stimulation induces stronger whisker protraction and stronger simple spike responses
A. Whisker traces of a representative mouse following air puff stimulation of the ipsilateral (*left panel*) and contralateral (*right panel*) whisker pad (see scheme in **B**). Despite a similar strength of stimulation, the protraction of the whiskers was larger upon contralateral stimulation (cf. Figure 2). **C.** Stacked line plots of the averaged whisker traces of 9 mice with the difference between the contralateral and ipsilateral stimulation depicted in the third column. **D.** Complex spike responses, on the other hand, were more prominent upon ipsilateral stimulation. **E.** The observation that increased simple spike firing correlates to enhanced whisker protraction (cf. Figure 6) was confirmed under these experimental conditions. * $p < 0.05$; *** $p < 0.001$. See also Data Source File.

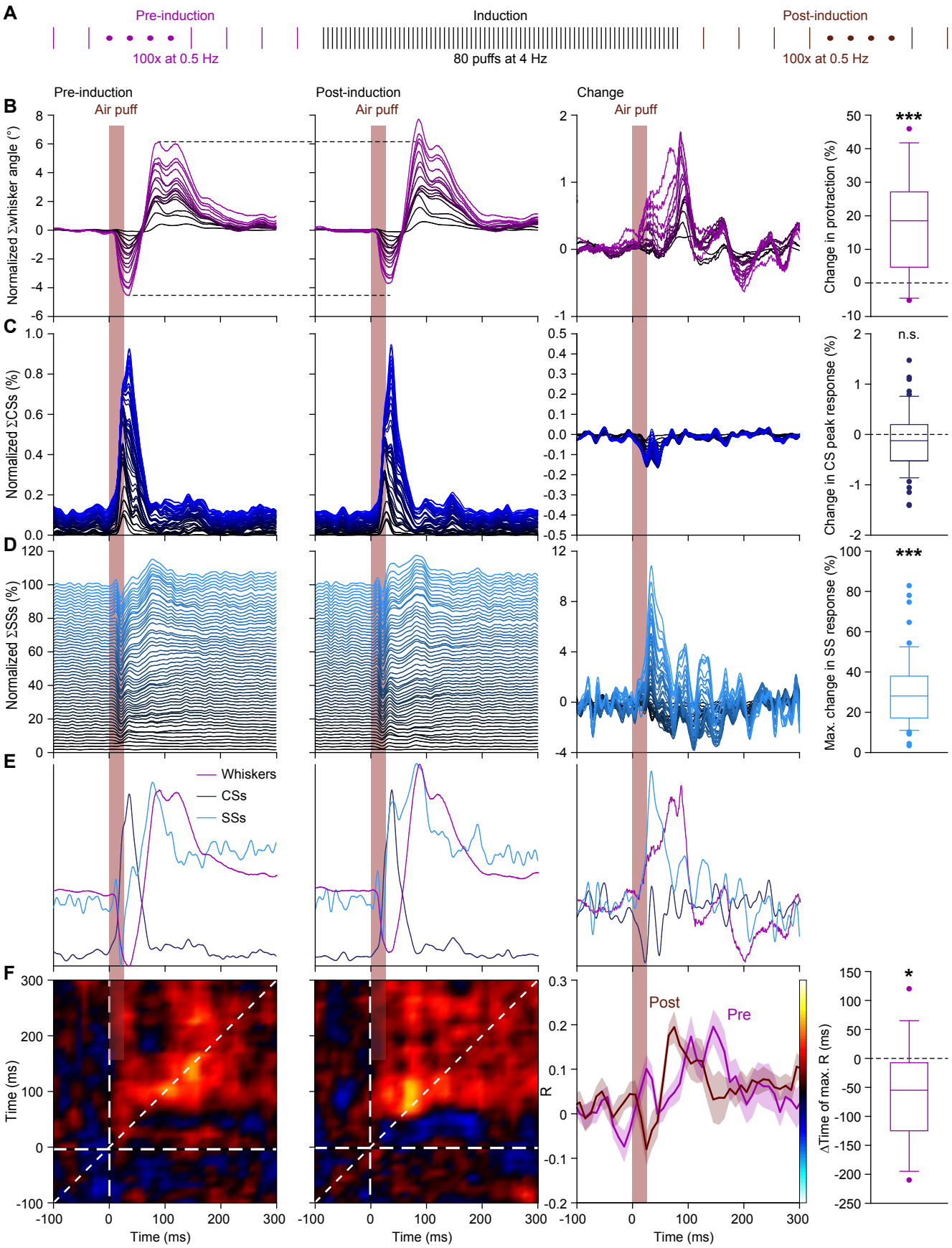

Figure 8 | 4 Hz tetanic stimulation leads to anticipation of the simple spike response and to stronger protraction of the whiskers

A. Induction protocol. Air puff stimulation at 0.5 Hz is used to characterize the impact of a brief period (20 s) of 4 Hz air puff stimulation. **B.** Stacked line plots (see Methods) showing the averaged whisker response before (1st column) and after (2nd column) 4 Hz sensory stimulation (n = 16 mice). The plots are sorted by increased protraction induced by 4 Hz tetanic stimulation (3rd column). Each color depicts one mouse. Plots are normalized so that the most intense color represents the average. 4 Hz tetanic stimulation leads to a more protracted form of whisker movement (4th column). Similar plots for complex spikes (**C**, showing little change) and simple spikes (**D**, showing a clear increase in firing, especially during the early phase of the response). For comparison, the averages are superimposed in **E** (for y-scaling and variations refer to **B**-**D**). Trial-by-trial analysis of 14 Purkinje cells before and after 4 Hz tetanic stimulation (cf. Figure 6C-D) highlighting the anticipation of simple spike firing (**F**). The x-axis is based upon the instantaneous simple spike firing frequency and the y-axis upon whisker angle. After induction, the maximal correlation (R) between simple spikes and whisker angle (along dashed 45° line) shifts to an earlier time point after the air puff (3rd column; shaded areas indicate SEM). In addition, a clear correlation is found with simple spike firing leading whisker movement (yellow/red area expands above the 45° line in 2nd column as compared to the left column). Scale bar of the correlation matrices (left and middle) is at the right of the 3rd column. ** $p < 0.01$; *** $p < 0.001$. See also Table S2 and Source Data File.

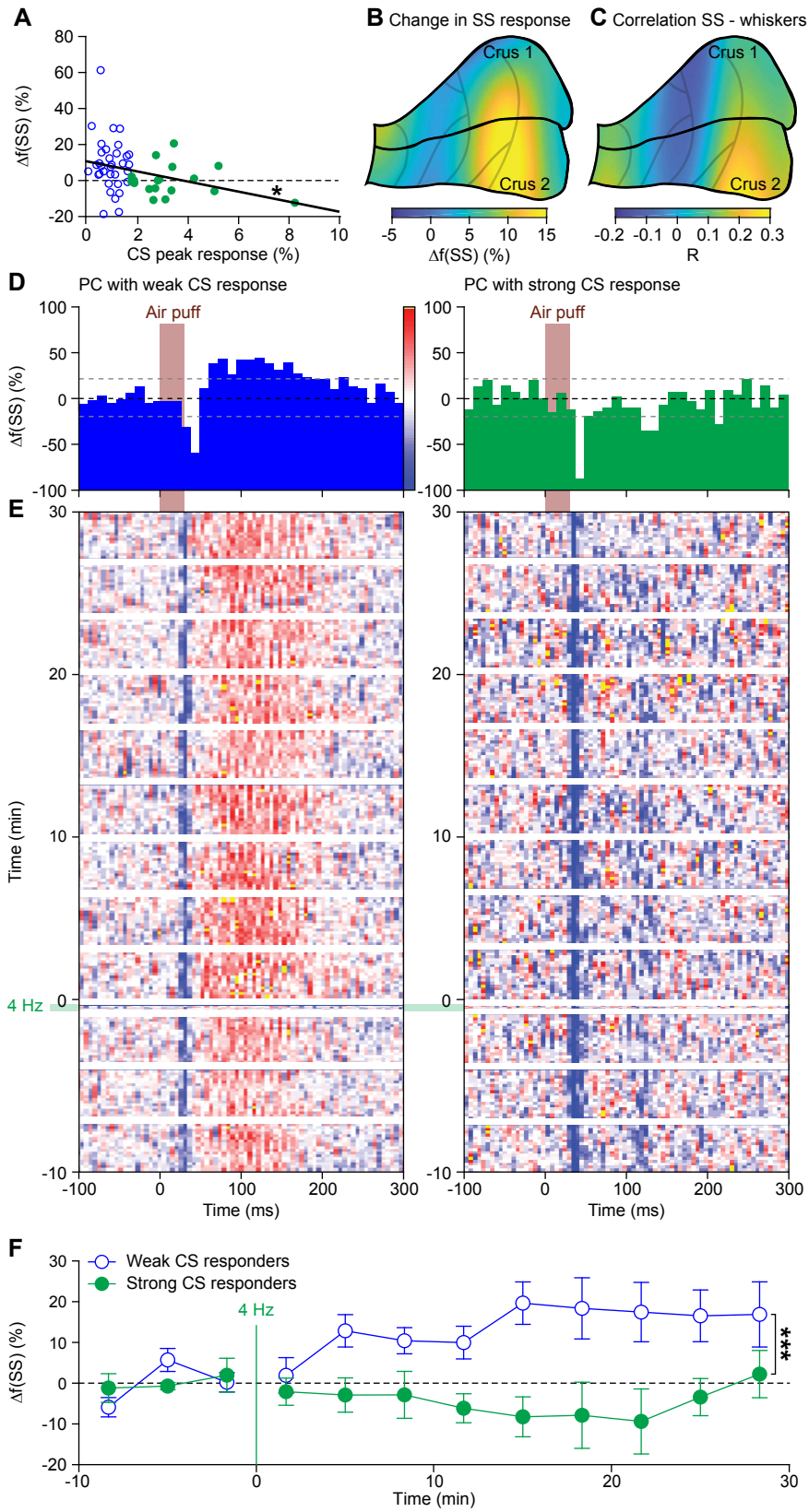

Figure 9 | 4 Hz tetanic stimulation specifically potentiates simple spike firing in Purkinje cells with weak complex spike responses

A. Repeated sensory stimulation (Figure 8A) induced an increase in simple spike response to whisker pad stimulation, but not in all Purkinje cells (PCs). There was a clear negative correlation between the strength of the complex spike (CS) response and the potentiation of the simple spike response. Overall, there was potentiation in the Purkinje cells with weak complex spike responses, but not in the strong CS responders (cf. Figure 3 - Figure supplement 1E). **B.** Heat map showing the anatomical distribution of the strength of the simple spike increase projected on the surface of crus 1 and crus 2. The 55 Purkinje cells were attributed to a rectangular grid. The average simple spike response strength was calculated per grid position and averaged between each grid position and its neighbor. The grey lines indicate the borders to the cerebellar zones (see Figure 3 - Figure supplement 2D). **C.** Heat map of the distribution of Purkinje cells based upon the correlation of their simple spike rate and whisker position (cf. Figure 6D). Note that the strongest increase of simple spike responses after 4 Hz tetanic stimulation occurs in the region that also displayed the strongest correlation between instantaneous simple spike rate and whisker position. **D.** Example PSTHs of the simple spike response to whisker pad air puff stimulation of representative Purkinje cells and how they changed over time, depicted as heat maps of the instantaneous simple spike frequency (**E**; see scale bar in **D**). The left column displays the data from a representative Purkinje cell with a weak complex spike response, the right column of one with a strong complex spike response. The induction period is indicated with "4 Hz". **F.** The number of simple spikes following an air puff stimulation increased in weakly responding Purkinje cells and this increase remained elevated until the end of the recording (at least 30 min). In contrast, this increase was not found in Purkinje cells with strong complex spike responses. * $p < 0.05$; ** $p < 0.01$; *** $p < 0.001$.

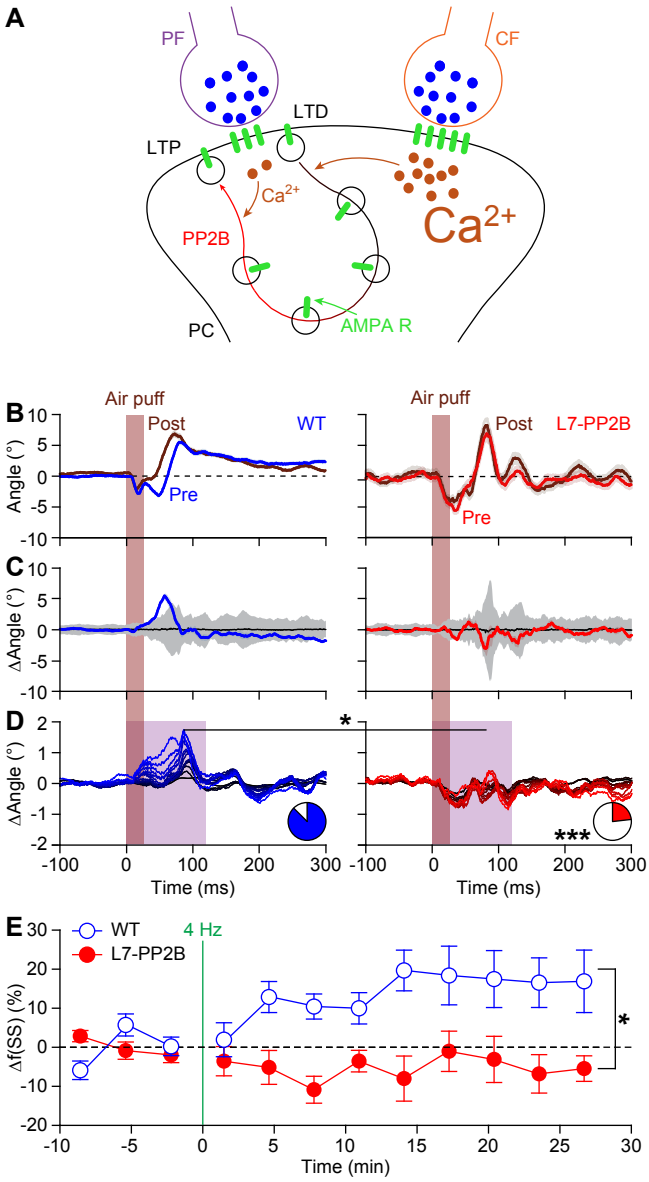

Figure 10 | Expression of PP2B in Purkinje cells is required for increased protraction and simple spike firing following 4 Hz tetanic stimulation
A. Schematic representation of the principal pathways regulating bidirectional plasticity at the parallel fiber (PF) to Purkinje cell (PC) synapses. The direction of PF-PC plasticity depends on the intracellular Ca^{2+} concentration ($[Ca^{2+}]_i$) that is largely determined by climbing fiber (CF) activity. Following CF activity, $[Ca^{2+}]_i$ raises rapidly and activates a phosphorylation cascade involving α-Ca^{2+}/calmodulin-dependent protein kinase II (CaMKIIA) and several other proteins eventually leading to internalization of AMPA receptors and consequently to long-term depression (LTD). PF volleys in the absence of CF activity, on the other hand, result in a moderate increase in $[Ca^{2+}]_i$, activating a protein cascade involving protein phosphatase 2B (PP2B) that promotes the insertion of new AMPA receptors into the postsynaptic density, thereby leading to long-term potentiation (LTP) of the PF-PC synapse. GluA3 subunits are part of the postsynaptic AMPA receptors. **B.** Example of a representative mouse with the averaged whisker movements before and after theta sensory stimulation, showing a stronger protraction afterwards, as evidenced by the differences between post- and pre-induction compared to a bootstrap analysis on the normal variation in whisker movements (**C**; shade: 99% confidence interval). Although also differences were observed in L7-PP2B mutants, these did generally not exceed the expected variations (*right*). **D.** In 14 out of 16 wild-type mice more protraction than expected was observed, against in only 3 out of 13 L7-PP2B mutant mice (pie charts). Stacked line plots of whisker movement differences between post- and pre-induction for all mice. The plots are normalized so that the brightest line indicates the average per genotype. **E.** In contrast to simple spike responses in WT mice, those in L7-PP2B KO mice could not be potentiated by our 4 Hz tetanic stimulation protocol. This effect was stable, also during longer recordings. For this analysis, we selected those with weak complex spike responses, as the PCs with a weak complex spike response did not show increased simple spike firing after 4 Hz tetanic stimulation (see Figure 9A).
* $p < 0.05$; ** $p < 0.01$; *** $p < 0.001$

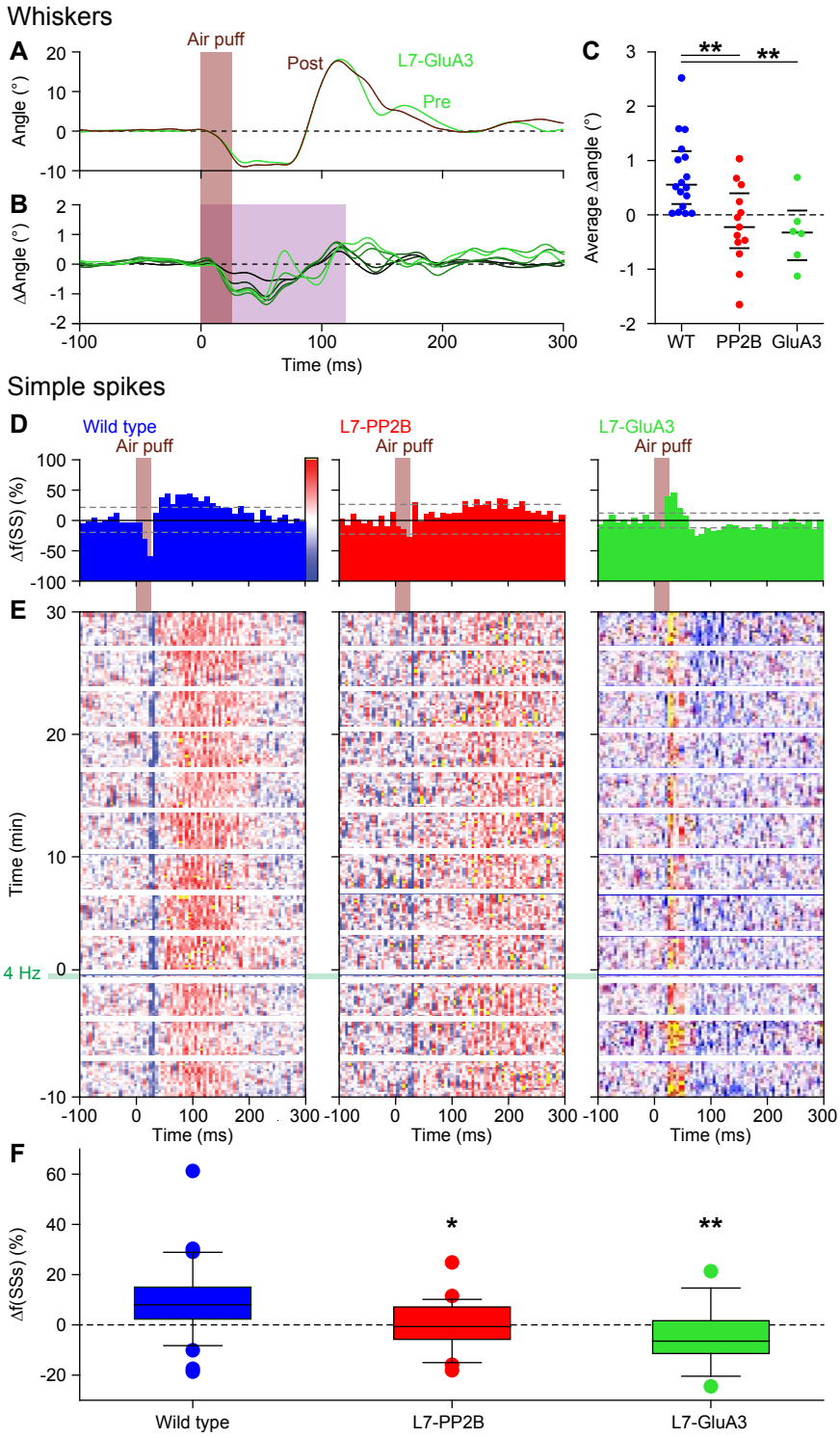

Figure 11 | Expression of AMPA receptor GluA3 subunits in Purkinje cells is required for increased protraction and simple spike firing following 4 Hz tetanic stimulation

A. Example of a representative L7-GluA3 mutant mouse with the averaged whisker movements before and after 4 Hz tetanic stimulation, showing similar degrees of protraction. **B.** Overall, 4 Hz tetanic stimulation did not result in stronger whisker protraction in L7-GluA3 mutant mice as observed in WT mice (see Figure 8). This is illustrated with a stacked line plot. **C.** Comparison of the average change in whisker angle over the 120 ms following the onset of the air puff shows enhanced protraction in WT (n = 16), but not in LTP-deficient mice - neither in L7-PP2B (n = 13) nor in L7-GluA3 (n = 6) mutants, pointing towards a central role for parallel fiber-to-Purkinje cell LTP for the enhanced protraction in WT mice following a brief period of 4 Hz tetanic stimulation. The horizontal lines indicate the medians and the 1st and 3rd quartiles. The lack of change in whisker protraction following 4 Hz tetanic stimulation was reflected in the lack of change in simple spike responses as illustrated in three representative Purkinje cells (cf. Figure 9D-E). On top are the peri-stimulus time histograms (**D**) followed by heat maps illustrating the instantaneous firing rate over time (**E**). The induction period is indicated with "4 Hz". **F.** Overall, WT Purkinje cells (n = 35) showed increased simple spike firing after 4 Hz stimulation, while those in L7-PP2B (n = 21) or L7-GluA3 (n = 13) mutant mice did not. For this analysis, we restricted ourselves to the Purkinje cells with weak complex spike responses as the Purkinje cells with strong complex spike responses did not show potentiation in the WT mice (see Figure 9A) and to the first 100 trials after induction. As shown in Figure 11E, the increase in simple spiking firing developed over time (in WT, but not in L7-PP2B mice). Directly following the induction period, the increase in simple spike firing was not yet maximal. * $p < 0.05$; ** $p < 0.01$. See also Source Data File.